Degenerate mixing of plasma waves on cold, magnetized single-species plasmas

M. W. Anderson, T. M. O'Neil, D. H. E. Dubin, and R. W. Gould

Citation: Phys. Plasmas **18**, 102113 (2011); doi: 10.1063/1.3646922
View online: http://dx.doi.org/10.1063/1.3646922
View Table of Contents: http://pop.aip.org/resource/1/PHPAEN/v18/i10
Published by the American Institute of Physics.

Degenerate mixing of plasma waves on cold, magnetized single-species plasmas

M. W. Anderson,[1] T. M. O'Neil,[1] D. H. E. Dubin,[1] and R. W. Gould[2]
[1]*Physics Department, University of California at San Diego, La Jolla, California 92093, USA*
[2]*California Institute of Technology, Mail Stop 128-95, Pasadena, California 91103, USA*

(Received 3 June 2011; accepted 12 September 2011; published online 24 October 2011)

In the cold-fluid dispersion relation $\omega = \omega_p/[1 + (k_\perp/k_z)^2]^{1/2}$ for Trivelpiece-Gould waves on an infinitely long magnetized plasma cylinder, the transverse and axial wavenumbers appear only in the combination $k_\perp/k_z$. As a result, for any frequency $\omega < \omega_p$, there are infinitely many degenerate waves, all having the same value of $k_\perp/k_z$. On a cold finite-length plasma column, these degenerate waves reflect into one another at the ends; thus, each standing-wave normal mode of the bounded plasma is a mixture of many degenerate waves, not a single standing wave as is often assumed. A striking feature of the many-wave modes is that the short-wavelength waves often add constructively along resonance cones given by $dz/dr = \pm(\omega_p^2/\omega^2 - 1)^{1/2}$. Also, the presence of short wavelengths in the admixture for a predominantly long-wavelength mode enhances the viscous damping beyond what the single-wave approximation would predict. Here, numerical solutions are obtained for modes of a cylindrical plasma column with rounded ends. Exploiting the fact that the modes of a spheroidal plasma are known analytically (the Dubin modes), a perturbation analysis is used to investigate the mixing of low-order, nearly degenerate Dubin modes caused by small deformations of a plasma spheroid. © *2011 American Institute of Physics*. [doi:10.1063/1.3646922]

I. BACKGROUND AND SUMMARY OF RESULTS

Figure 1 shows a schematic diagram of a single-species plasma that is confined in a Penning-Malmberg trap.[1] A conducting cylinder is divided into three sections, and the plasma resides in the central grounded section, with radial confinement provided by a uniform axial magnetic field ($\mathbf{B} = B\hat{\mathbf{z}}$) and axial confinement by voltages applied to the outer sections of the cylinder. These plasmas routinely come to a state of thermal equilibrium in the trap and are routinely cooled to the cryogenic temperature range.[2] The plasma configuration is then particularly simple; the density is constant out to some surface of revolution and there drops to zero.[3] This paper discusses the normal modes of plasma oscillation for these cold equilibrium plasmas. Of course, cold-fluid theory provides a good description of these modes.

At first glance, the problem sounds straightforward: find the longitudinal modes of oscillation of a uniformly magnetized, uniform-density, bounded plasma in cold-fluid theory. However, we will see that the problem is subtle and that there is some confusion in the literature.

The origin of the difficulty is the peculiar dispersion relation for plasma waves in a cold magnetized plasma,

$$\omega = \frac{k_z \omega_p}{\sqrt{k_z^2 + k_\perp^2}}, \tag{1}$$

where ω is the wave frequency, ω_p is the plasma frequency in the unperturbed plasma, k_z is the wavenumber along the magnetic field, and $k_\perp$ is the wavenumber transverse to the field. Note that a wave with wavenumbers $(k_z, k_\perp)$ has the same frequency as a wave with wavenumbers $(k_z', k_\perp')$ if $k_z'/k_\perp' = k_z/k_\perp$ thus, each wave has the same frequency as infinitely many other waves. Upon reflection from the boundaries, an incident wave typically mixes with other waves sharing the same frequency, and consequently, each normal mode is a complicated many-wave structure.

A toy problem illustrates the issues. Consider a two dimensional slab of uniform-density plasma that occupies the bounded domain given by $0 \le x \le a$ and $0 \le z \le b$, and assume a strong magnetic field in the z-direction. The potential for a mode oscillating with frequency ω satisfies the equation

$$\frac{\partial^2 \delta\varphi_\omega}{\partial x^2} + \left(1 - \frac{\omega_p^2}{\omega^2}\right)\frac{\partial^2 \delta\varphi_\omega}{\partial z^2} = 0. \tag{2}$$

Suppose that the plasma is bounded on all sides by a perfect conductor, the potential is zero at the boundaries. In this case, a set of normal modes and frequencies is given by

$$\delta\varphi_\omega(x,z) = \sin\left(\frac{m\pi x}{a}\right)\sin\left(\frac{n\pi x}{b}\right), \tag{3}$$

$$\omega_{mn} = \frac{(n\pi/b)\omega_p}{\sqrt{(m\pi/a)^2 + (n\pi/b)^2}}, \tag{4}$$

where m and n are integers. For any mode (m,n), there are an infinite number of exactly degenerate modes (m',n') where $n'/m' = n/m$. Each mode can be decomposed into a pair of waves propagating in opposite directions along the magnetic field and reflecting at the boundaries, but for this particular geometry, there is no mixing since the sine functions are orthogonal on the boundary surfaces. However, if the boundary were deformed, the orthogonality would be destroyed, and reflections would mix degenerate modes, yielding more complicated many-wave modes.

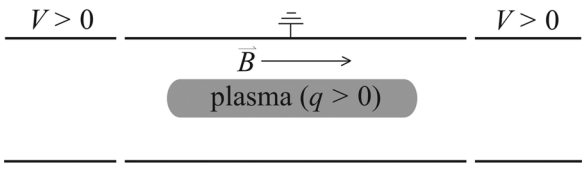

FIG. 1. Schematic diagram of a finite-length single-species plasma column confined in a Penning-Malmberg trap. Axial confinement is electrostatic, provided by an electric potential, V, applied to the outer cylindrical electrodes; radial confinement is provided by an axial magnetic field. The confinement scheme depicted here is for positively charged particles.

It is interesting to construct an alternate representation of the degenerate modes. For any frequency, the mode equation (2) admits characteristic solutions of the form $\delta\varphi_\omega = \delta[z \pm (\omega_p^2/\omega^2 - 1)^{1/2} x + c]$, where c is an arbitrary constant. These solutions can be thought of as a line or ray at slope $dz/dx = \pm(\omega_p^2/\omega^2 - 1)^{1/2}$. For the mode frequencies given by Eq. (4), an assembly of such rays can be arranged end to end, so that the assembly closes on itself. The sign of the ray changes upon reflection from the boundary, so that the boundary condition on the wall is satisfied. Figure 2 shows a parallelogram-shaped assembly for the degenerate mode frequency corresponding to $n/m = 1$. There are an infinite number of such parallelograms with sides of different lengths, and this set is an alternative representation of the sinusoidal degenerate modes of Eq. (3) for which $n/m = 1$. Similar ray-like representations can be constructed for any other set of degenerate modes—that is, for any other value of the ratio n/m. Interestingly, if the rectangular plasma boundary is deformed slightly, all of the degenerate sinusoidal modes are mixed, but a given ray-like mode is only modified if the boundary is moved at the points at which the ray makes contact.

This picture is modified somewhat in cylindrical geometry. For example, for a uniform-density plasma bounded by a cylindrical conducting wall at $r = a$ and flat conducting walls at $z = 0$ and $z = b$, the mode degeneracies are only

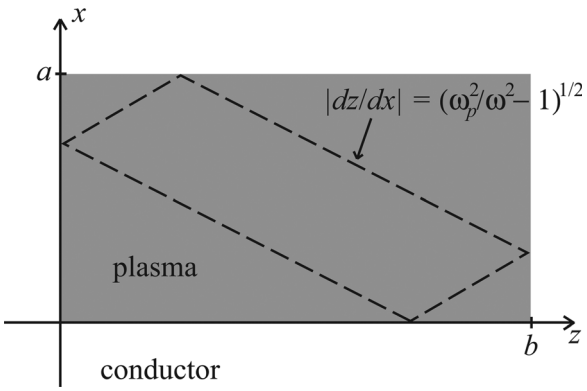

FIG. 2. An example of a ray-like mode on a magnetized plasma slab of rectangular cross-section, surrounded by a perfect conductor. The mode potential is a sum of four Dirac delta functions, each of which is peaked along one side of the dashed parallelogram. Delta functions corresponding to adjacent sides enter the sum with opposite signs so that the condition of vanishing potential is satisfied along the boundary. There are an infinite number of other ray-like modes with the same frequency as the mode depicted here. The set of ray-like modes is complimentary to the set of modes that are sinusoidal in x and z.

approximate. Furthermore, the ray-like solutions are replaced by more complicated functions that are peaked along resonance cones with slope[4] $dz/dr = \pm(\omega_p^2/\omega^2 - 1)^{1/2}$. A crucial difference is that the cylindrical functions are not entirely localized along these cones. Nevertheless, the basic ideas illustrated by the rectangular toy problem persist. In numerical studies of the normal modes for a long, cylindrical plasma column in a Penning-Malmberg trap, we will find complicated many-wave normal modes, with the waves often adding to produce conical structures with slope $dz/dr = \pm(\omega_p^2/\omega^2 - 1)^{1/2}$.

We emphasize that the mixing described here is a low-temperature phenomenon, requiring that the cold-fluid dispersion relation be valid for axial and transverse wavelengths much shorter than the dimensions of the plasma. The condition for validity of the cold-fluid dispersion relation is that $(k_\perp^2 + k_z^2)^{1/2}\lambda_D \ll 1$; otherwise, kinetic effects such as Landau damping modify the dispersion relation, spoiling the degeneracy that underlies the mixing. Using the laser cooling technique, experimentalists regularly achieve Debye lengths that are small compared with the plasma dimensions, and in this regime, mixing should be observable. For example, a recent experiment on Mg^+ plasmas achieved a temperature of 10^{-3} eV at a density of 2×10^7 cm^{-3}, corresponding to a Debye length of 5×10^{-3} cm; the plasma radius in this experiment was on the order of 1 cm.[5]

With this background, we now return to the discussion of normal modes for a cold equilibrium plasma in a Penning-Malmberg trap. An important difference between this problem and the toy problem is that vacuum separates the plasma from the conducting wall. For the simple case of a mode with azimuthal mode number zero, the mode equation is given by

$$\frac{1}{r}\frac{\partial}{\partial r} r \frac{\partial \delta\varphi_\omega}{\partial r} + \frac{\partial}{\partial z}\left[1 - \frac{\omega_p^2(r,z)}{\omega^2}\right]\frac{\partial \delta\varphi_\omega}{\partial z} = 0, \qquad (5)$$

where $\omega_p^2(r,z) = \omega_p^2 =$ *constant* inside the plasma and $\omega_p^2(r,z) = 0$ in the vacuum. The mode potential vanishes on the trap wall and as $z \to \pm\infty$.

Historically, two geometrical limits have been emphasized. In the first limit, pioneered by the atomic physics community, the plasma is small compared to the radius of the cylindrical conductor and resides in a quadratic trap potential. The surface of revolution defining the shape of the plasma is spheroidal in this limit.[6] Using spheroidal coordinates, exact analytic expressions for the normal modes can be found, and images of modes in Be + plasmas corroborate these results.[7,8] However, these modes have many near degeneracies, and one expects that a deformation of the spheroidal boundary will mix these modes.

In the second limit, more familiar to plasma physicists, the plasma is long compared to the radius of the conducting cylinder and takes the shape of a finite-length cylinder with rounded ends. The more complicated shape of these longer plasmas prevents an analytic description of the modes. However, the solution by Trivelpiece and Gould (TG) for waves on a cold, magnetized, infinitely long plasma cylinder provides a useful benchmark for theoretical studies of modes

on a finite-length plasma cylinder.[9] Previous theory has argued that, to a good approximation, each mode is a single standing TG wave with the axial wavenumber quantized to fit the length of the plasma column. Moreover, for the case of warm plasmas with significant kinetic effects, experimental observations are consistent with this simple picture.[10] In contrast, our numerical solution based on cold-fluid theory shows that each mode involves many TG waves, which often add to produce conical structures at the expected slope, $dz/dr = \pm(\omega_p^2/\omega^2 - 1)^{1/2}$.

The dispersion relation for the TG waves is given by Eq. (1), but with the transverse wavenumber $k_\perp$ quantized to discrete values, each corresponding to a different solution to the differential equation for the radial dependence of the wave. Upon reflection at the end of the column, a given TG wave reflects not only into its backward-propagating counterpart, but also into other waves with different radial wavefunctions.[11] Note that when ω and $k_\perp$ are specified, Eq. (1) chooses the value of k_z. The value of k_z is important in determining the extent to which a wave participates in the mode. If, after a complete circuit of two reflections, the wave adds in a phase with itself (say, to produce a standing wave), then that wave will tend to play a significant role in the mode. Such approximate standing waves here play the role of the exactly degenerate modes in the toy problem.

The numerical method employed here is easiest to understand for the idealized case where the plasma column has flat ends—that is, where the plasma is a perfect right circular cylinder as shown in Fig. 3(a). In this case, the plasma has a well-defined length, L and we take the plasma to be centered on the origin, so that the ends of the plasma lie at $z = \pm L/2$. The dashed lines in Fig. 3(a) divide the confinement region axially into a central region where the plasma resides and two adjacent vacuum regions. Following Prasad and O'Neil,[11] we expand the mode potential in the central region in an infinite series of TG waves, all having the same frequency, ω—the unknown frequency of the mode—but different axial and transverse wavenumbers, k_z and $k_\perp$. Each of these waves satisfies the mode equation for a mode with frequency ω as well as the boundary condition on the wall, and each can be expressed analytically. In the vacuum region $z > L/2$, we express the mode potential in an infinite series of cylindrical harmonics of the form $J_0(\chi_{0n} r/R) \exp[-\chi_{0n}(z - L/2)/R]$, where R is the radius of the conducting cylinder, χ_{0n} is the nth zero of the Bessel function $J_0(x)$, and n is a positive integer. For the vacuum region $z < -L/2$, there is simply a sign change in the argument of the exponential (and an overall sign change in the case of odd modes). The three series satisfy the mode equation in the three regions as well as the boundary conditions on the wall and at $z \to \pm\infty$, and the numerical task is to find a frequency ω and to choose the coefficients in the series, so that the solutions match properly across the surfaces separating these regions. The mode potential and the normal component of the electric displacement vector must be continuous across these surfaces.

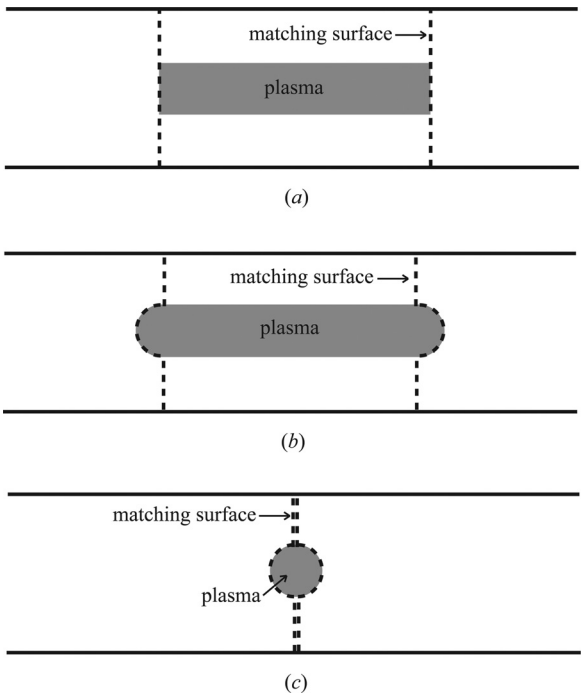

FIG. 3. Three idealized plasma shapes for which the modes of oscillation are calculated: (a) a cylinder with flat ends, (b) a cylinder with spheroidal ends, and (c) a spheroid. In each of the three regions separated by the dashed curves, we express the mode potential as a linear combination of functions that satisfy the mode equation and boundary conditions in that particular region. The numerical task is to choose the coefficients in each linear combination, so that the mode potential and the normal derivative of the electric displacement match at the boundary surfaces shown here as dashed curves.

An advantage of this numerical method is that it explicitly identifies the extent to which each TG wave participates in a given normal mode. Also, use of the known TG wave solutions and vacuum solutions effectively reduces the dimension of the numerical task. Matching on the boundary surface involves N unknowns, whereas a numerical solution on a grid spanning r and z would involve N^2 unknowns.

For the simple case of flat ends, the matching task is facilitated by the orthogonality of both the Bessel functions and the TG radial wavefunctions on the flat matching surfaces [the dashed lines in Fig. 3(a)]. Note, however, that the Bessel functions are not orthogonal to the TG radial wavefunctions; indeed, it is the lack of orthogonality that gives rise to mixing upon reflection. Each TG wave couples to many vacuum solutions, and these couple back to different TG waves. In contrast with the toy problem, the plasma ends need not be deformed to get wave mixing.

Of course, numerical solution of the matching conditions requires that the three series be truncated at a finite number of terms, and here a difficulty arises for the idealization of a flat end. We do not find convergence of the solution, in that TG waves of arbitrarily large wavenumber appear to participate significantly in each mode.

Figure 3(b) shows a more realistic plasma with spheroidal ends that fit smoothly onto the central cylindrical section of the plasma. Here, the matching surfaces that separate the central region containing the plasma from the adjacent vacuum regions are no longer flat but extend outward to follow the end-shape of the plasma [the dashed curves in Fig. 3(b)]. Again we expand the mode potential in three series for the three regions, but here we lose the orthogonality of the Bessel functions and of the TG radial wavefunctions on the

matching surfaces. The matching is carried out by choosing the frequency and the coefficients in the series to minimize the mean-squared error in matching at a large number of sample points on the matching surface. Fortunately, the rounding of the ends suppresses the coupling to large-wavenumber components, and we find convergent solutions.

By taking the central cylindrical section of the plasma to be much shorter than the spheroidal end-caps, we obtain a plasma that is nearly spheroidal in shape, as illustrated in Fig. 3(c). Then, by taking the radius of the trap to be large in comparison with the dimensions of the plasma, we approach the limit in which analytic expressions for the modes are known.[7] In this range of parameters, modes obtained using our numerical method bear close resemblance to those predicted by the analytic expressions. However, for these nearly spheroidal plasmas, convergence is too slow to resolve fine-scale details of the modes.

For a nearly spheroidal plasma, perturbation theory provides a more instructive approach; the modes of a perfectly spheroidal plasma provide a natural set of basis functions for this perturbation analysis. The basis functions become mixed when small deformations of the spheroidal plasma boundary are introduced, and we obtain a general expression for the coupling. In the neighborhood of particular values of the plasma aspect ratio where multiple low-order basis functions are degenerate, the mixing can be of order unity. However, such strong mixing is limited by a selection rule; basis functions with disparate modenumbers will not be strongly mixed unless the perturbed plasma boundary exhibits fine-scale ripples.

When viscosity is introduced, a signature of the predicted wave-mixing is that the least damped modes of the cold plasma cylinder damp more quickly than one would expect based on the assumption that the mode is a single standing TG wave. The reason for the enhanced damping is that the viscous momentum flux underlying the damping is intensified by the presence of steep momentum gradients—i.e., high wavenumbers—in the mixed mode. We investigate viscous damping in the limit where viscous effects can be treated as a perturbation to Eq. (5). To first order in viscosity, each mode damps with a rate given by a quadratic form that acts on the zero-order (inviscid) mode. We evaluate this expression for one of the numerically calculated modes and compare with the rate obtained by approximating the mode as a single TG wave. The single-wave approximation underestimates the damping rate by roughly an order of magnitude.

The organization of the paper is as follows: in Sec. II, we introduce the equations of motion for the cold, magnetized plasma; in Sec. III, we review the TG solutions for an infinitely long plasma column; in Sec. IV, we seek the modes of a finite-length plasma column with flat ends; in Sec. V, modes of a finite-length plasma column with rounded ends are obtained numerically; in Sec. VI, the mixing of modes on a nearly spheroidal plasma is investigated using perturbation theory; and in Sec. VII, viscous damping is discussed.

II. COLD-FLUID EQUATIONS OF MOTION

As an approximation to the Penning-Malmberg trap configuration shown in Fig. 1, we assume that mode potential satisfies the boundary conditions $\delta\varphi = 0$ at $r = R$ and at $z \to \pm\infty$, where R is the radius of the conducting wall of the trap. For azimuthally symmetric modes, Poisson's equation takes the form

$$\frac{1}{r}\frac{\partial}{\partial r}r\frac{\partial\delta\varphi}{\partial r} + \frac{\partial^2\delta\varphi}{\partial z^2} = -4\pi q\delta n, \tag{6}$$

where $\delta\varphi$ is the mode potential, δn is the corresponding density perturbation, and q is the charge of a single particle.

In accord with the experiments that we have in mind, we assume that the axial magnetic field in the trap is sufficiently large that the drift approximation is justified. In cold-fluid theory, small azimuthally symmetric perturbations then evolve in time following the linearized continuity and momentum equations,

$$\frac{\partial\delta n}{\partial t} + \frac{\partial}{\partial z}(n_0\delta V_z) = 0, \tag{7}$$

$$mn_0\frac{\partial\delta V_z}{\partial t} = -qn_0\frac{\partial\delta\varphi}{\partial z}, \tag{8}$$

where δV_z is the perturbed fluid velocity associated with the mode, $n_0(r,z)$ is the unperturbed density, and m is the particle mass.

Seeking normal-mode solutions to Eqs. (6)–(8), we assume that the perturbation oscillates with frequency ω,

$$\begin{Bmatrix}\delta n(r,z,t)\\ \delta V_z(r,z,t)\\ \delta\varphi(r,z,t)\end{Bmatrix} = \mathrm{Re}\left[e^{-i\omega t}\times\begin{Bmatrix}\delta n_\omega(r,z)\\ \delta V_{z,\omega}(r,z)\\ \delta\varphi_\omega(r,z)\end{Bmatrix}\right] \tag{9}$$

and substitute, obtaining

$$\frac{1}{r}\frac{\partial}{\partial r}r\frac{\partial\delta\varphi_\omega}{\partial r} + \frac{\partial^2\delta\varphi_\omega}{\partial z^2} = -4\pi q\delta n_\omega, \tag{10}$$

$$-i\omega\delta n_\omega + \frac{\partial}{\partial z}(n_0\delta V_{z,\omega}) = 0, \tag{11}$$

$$-i\omega mn_0\delta V_{z,\omega} = -qn_0\frac{\partial\delta\varphi_\omega}{\partial z}. \tag{12}$$

Equations (10)–(12) can be combined to give

$$\frac{1}{r}\frac{\partial}{\partial r}r\frac{\partial\delta\varphi_\omega}{\partial r} + \frac{\partial}{\partial z}\left[1 - \frac{\omega_p^2(r,z)}{\omega^2}\right]\frac{\partial\delta\varphi_\omega}{\partial z} = 0, \tag{13}$$

where $\omega_p^2(r,z) = 4\pi q^2 n_0(r,z)/m$. Equation (13) represents a generalized eigenvalue problem, since typically both $\delta\varphi_\omega$ and ω are unknown.

Multiplication of Eq. (13) by $\delta\varphi_\omega$ and integration over the interior of the trap gives a formal expression for the mode frequency in terms of the mode potential,[12]

$$\omega^2 = \frac{\int rdrdz\omega_p^2(r,z)(\partial\delta\varphi_\omega/\partial z)^2}{\int rdrdz[(\partial\delta\varphi_\omega/\partial z)^2 + (\partial\delta\varphi_\omega/\partial r)^2]}, \tag{14}$$

where integration by parts has been employed. It follows from this formula that the allowed mode frequencies are real

and bounded by the plasma frequency; that is, $0 \le \omega^2 \le \max[\omega_p^2(r,z)] = \omega_p^2$.

Alternatively, one can derive an integral equation[13] for the z-component of the mode electric field, $\delta E_{z,\omega} = -\partial\delta\varphi_\omega/\partial z$, by inverting Poisson's equation with the Green's function, $G(r,z|r',z')$, defined by the conditions

$$\frac{1}{r}\frac{\partial}{\partial r}r\frac{\partial G}{\partial r}+\frac{\partial^2 G}{\partial z^2}=\frac{\delta(r-r')\delta(z-z')}{r}, \tag{15}$$

$$G|_{r=R}=G|_{|z-z'|\to\infty}=0. \tag{16}$$

In terms of the Green's function, Eq. (10) can be recast in the form

$$\delta\varphi_\omega(r,z)=-4\pi q\int r'dr'dz'\delta n_\omega(r',z')G(r,z|r',z'). \tag{17}$$

Equations (11) and (12) give the perturbed density in terms of the electric field,

$$4\pi q\delta n_\omega=-\frac{\partial}{\partial z}\left[\frac{\omega_p^2(r,z)}{\omega^2}\delta E_{z,\omega}\right]. \tag{18}$$

Inserting this expression in Eq. (17), integrating by parts, and taking the partial derivative with respect to z, one obtains the integral equation

$$\omega^2\delta E_{z,\omega}(r,z)=-\int r'dr'dz'\omega_p^2(r',z')\frac{\partial G}{\partial z\partial z'}\delta E_{z,\omega}(r',z'). \tag{19}$$

Unlike Eq. (13), Eq. (19) constitutes a linear eigenvalue problem, $-\omega^2$ being the eigenvalue, and $\delta E_{z,\omega}$, the eigenfunction. Furthermore, the integral operator on the right-hand-side is self-adjoint with respect to the inner product $(f_1,f_2)\equiv\int rdrdz\omega_p^2(r,z)f_1f_2$. It follows that all mode frequencies are real and that for any two modes with distinct frequencies ω and ω' the axial electric fields are orthogonal inside the plasma,

$$\int rdrdz\omega_p^2(r,z)\delta E_{z,\omega}(r,z)\delta E_{z,\omega'}(r,z)=0 \quad (\omega\neq\omega'). \tag{20}$$

While the integral equation (19) is equivalent to the differential equation (13) (with boundary conditions), it should be emphasized that $\delta E_{z,\omega}$—not $\delta\varphi_\omega$—is the true eigenfunction. For a mode that consists of many component waves, this distinction is important, since it is easy to underestimate the degree of the mixing when viewing a plot of the mode potential (see Figs. 5 and 8). For example, a wave with axial wavenumber k_z that appears with amplitude A in the z-component of the mode electric field will appear with amplitude A/k_z in the mode potential, since $\delta E_{z,\omega}=-\partial\delta\varphi_\omega/\partial z$. In this sense, large axial wavenumbers are suppressed relative to smaller wavenumbers in the mode potential. In contrast, the density gives an exaggerated impression of the mixing; a wave which appears with amplitude A in the z-component of the mode electric field will appear with amplitude $(k_\perp^2|k_z^2)A/k_z$ in the mode density.

III. TRIVELPIECE-GOULD WAVES

Before considering modes of a finite-length plasma cylinder, we present the solutions of Eq. (13) obtained by Trivelpiece and Gould for the case of an infinitely long cylinder.[9] In this case, Eq. (13) simplifies to

$$\frac{1}{r}\frac{\partial}{\partial r}r\frac{\partial\delta\varphi_\omega}{\partial r}+\left[1-\frac{\omega_p^2(r)}{\omega^2}\right]\frac{\partial^2\delta\varphi_\omega}{\partial z^2}=0, \tag{21}$$

which is separable. Specifically, for any real ω, there exist an infinite number of degenerate solutions of the form

$$\delta\varphi_\omega(r,z)=\psi_m^{TG}(\omega;r)e^{\pm ik_m z}. \tag{22}$$

Substitution into Eq. (21) yields a differential equation for the radial dependence, $\psi_m^{TG}(\omega;r)$,

$$\frac{1}{r}\frac{d}{dr}r\frac{d\psi_m^{TG}(\omega;r)}{dr}-k_m^2\left[1-\frac{\omega_p^2(r)}{\omega^2}\right]\psi_m^{TG}(\omega;r)=0. \tag{23}$$

In thermal equilibrium, the radial plasma density profile, $n_0(r)$, is nearly constant out to some radius and then abruptly falls off on the scale of the Debye length. Following Trivelpiece and Gould, we take an unperturbed density profile that is constant out to some radius, a, and zero outside this radius,

$$n_0(r)=n_0H(r-a), \tag{24}$$

where $H(x)$ is the Heaviside step function. This choice corresponds to an equilibrium density profile in the limit of zero temperature. A finite-temperature equilibrium density profile in place of the approximation (24) would necessitate numerical solution of Eq. (23), but the qualitative behavior of these solutions (e.g., oscillatory out to some radius; monotonically decreasing outside this radius) would be the same.

With the assumption of a step-function density profile, Eq. (23) becomes a Bessel equation in the domain $r<a$ and a modified Bessel equation in the domain $a<r<R$. Making use of the boundary condition $\delta\varphi=0$ at $r=R$ and requiring that $\delta\varphi$ be continuous at $r=a$, one finds solutions of the form

$$\psi_m^{TG}(\omega;r)\sim\begin{cases}\dfrac{J_0\left(k_m r\sqrt{\omega_p^2/\omega^2-1}\right)}{J_0\left(k_m a\sqrt{\omega_p^2/\omega^2-1}\right)} & r\le a\\ \dfrac{I_0(k_m r)K_0(k_m R)-I_0(k_m R)K_0(k_m r)}{I_0(k_m a)K_0(k_m R)-I_0(k_m R)K_0(k_m a)} & a<r\le R.\end{cases} \tag{25}$$

The wavenumber $k_m=k_m(\omega)$ is given by the mth nonnegative solution to the equation

$$\sqrt{\omega_p^2/\omega^2-1}\,\frac{J_1\left(ka\sqrt{\omega_p^2/\omega^2-1}\right)}{J_0\left(ka\sqrt{\omega_p^2/\omega^2-1}\right)}+\frac{I_0'(ka)K_0(kR)-I_0(kR)K_0'(ka)}{I_0(ka)K_0(kR)-I_0(kR)K_0(ka)}=0, \tag{26}$$

which comes from the requirement that $\partial\delta\varphi/\partial r$ be continuous at $r = a$. These are the azimuthally symmetric Trivelpiece-Gould waves. By defining the transverse wavenumber $k_{\perp,m} \equiv k_m(\omega_p^2/\omega^2 - 1)^{1/2}$, one recovers the dispersion equation (1).

In addition to the Trivelpiece-Gould waves, there exists another class of solutions to Eq. (21) of the form[11]

$$\delta\varphi_\omega(r,z) = \psi_m^A(\omega;r)e^{\pm\kappa_m z}. \tag{27}$$

For these solutions, the radial dependence is given by

$$\psi_m^A(\omega;r) \sim \begin{cases} \dfrac{I_0\left(\kappa_m r\sqrt{\omega_p^2/\omega^2-1}\right)}{I_0\left(\kappa_m a\sqrt{\omega_p^2/\omega^2-1}\right)} & r \le a \\ \dfrac{J_0(\kappa_m r)N_0(\kappa_m R) - J_0(\kappa_m R)N_0(\kappa_m r)}{J_0(\kappa_m a)N_0(\kappa_m R) - J_0(\kappa_m R)N_0(\kappa_m a)} & a < r \le R, \end{cases} \tag{28}$$

where κ_m is the mth nonnegative solution to the equation

$$\sqrt{\omega_p^2/\omega^2-1}\,\frac{I_1\left(\kappa a\sqrt{\omega_p^2/\omega^2-1}\right)}{I_0\left(\kappa a\sqrt{\omega_p^2/\omega^2-1}\right)} + \frac{J_0'(\kappa a)N_0(\kappa R) - J_0(\kappa R)N_0'(\kappa a)}{J_0(\kappa a)N_0(\kappa R) - J_0(\kappa R)N_0(\kappa a)} = 0. \tag{29}$$

We will refer to these solutions as "annular solutions," since they are localized in the annular vacuum region $a < r < R$. Because the annular solutions become exponentially large as $z \to \pm\infty$, they are typically ignored in the theory of the infinitely long cylinder; however, we will need these solutions when we solve for modes of a finite-length plasma cylinder.

The functions $\psi_m^{TG}(\omega;r)$ and $\psi_m^A(\omega;r)$ are mutually orthogonal on the interval $0 < r < R$ with weight function $\varepsilon(\omega,r) \equiv 1 - \omega_p^2(r)/\omega^2$; we choose the normalization so that[11]

$$\int_0^R r dr \varepsilon(\omega,r)\psi_m^{TG}(\omega;r)\psi_{m'}^{TG}(\omega;r) = -\frac{R^2}{2}\delta_{mm'} \tag{30}$$

and

$$\int_0^R r dr \varepsilon(\omega,r)\psi_m^{A}(\omega;r)\psi_{m}^{A}(\omega;r) = \frac{R^2}{2}\delta_{mm'}. \tag{31}$$

The difference in sign ensures that both $\psi_m^{TG}(\omega;r)$ and $\psi_m^A(\omega;r)$ are real-valued functions, since the function $\varepsilon(\omega,r)$ is negative inside the plasma, where the functions $\psi_m^{TG}(\omega;r)$ are localized, and positive outside the plasma, where the functions $\psi_m^A(\omega;r)$ are localized. Several of the functions $\psi_m^{TG}(\omega;r)$ and $\psi_m^A(\omega;r)$ are plotted in Fig. 4 for $R = 1$, $a = 1/2$, and $\omega/\omega_p = 1/10$.

IV. MODES OF A PLASMA COLUMN WITH FLAT ENDS

We now search for modes of a finite-length plasma cylinder. Jennings *et al.* approached this problem by discretizing equation (13), while Rasband *et al.* employed a finite-element method.[12,14] Following Prasad and O'Neil,[11] we choose to represent each mode as a linear combination of the TG and annular solutions discussed in Sec. III. This approach manifests the mixing of degenerate waves.

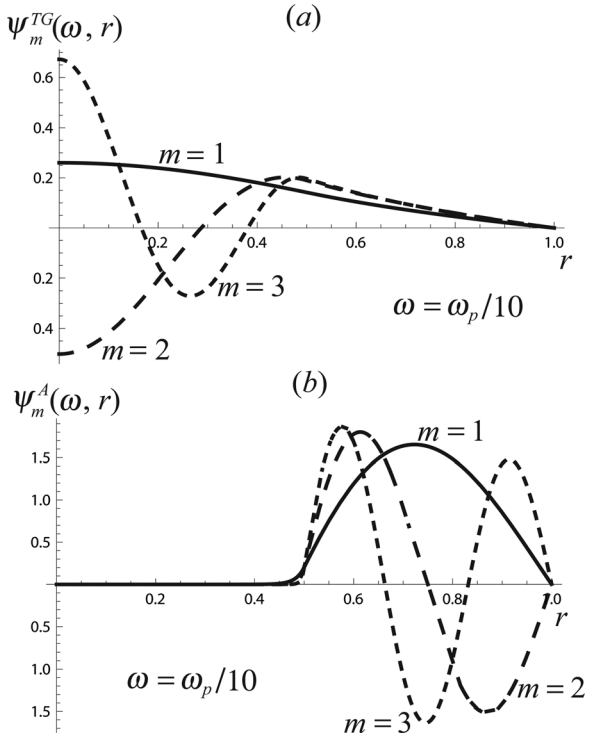

FIG. 4. Several of the functions $\psi_m^{TG}(\omega;r)$ and $\psi_m^A(\omega;r)$ plotted for the parameter values $\omega/\omega_p = 0.1$, $a = 0.5$, and $R = 1$. These functions give the radial dependence of the Trivelpiece-Gould and annular solutions on an infinitely long plasma cylinder.

In this section, we focus on a well-known model which takes the unperturbed plasma density to be constant inside a right-circular cylinder of radius a and length L and zero outside this cylinder [Fig. 3(a)],

$$n_0(r,z) = n_0 H(r-a)H(|z| - L/2). \tag{32}$$

In this case, although the Trivelpiece-Gould and annular solutions are no longer global solutions to Eq. (13), they still satisfy this equation in the region $|z| < L/2$. We assume that the mode potential in this region can be expressed as a linear combination of these solutions,

$$\delta\varphi_\omega(r,z) = \sum_{m=1}^{\infty} B_m\psi_m^{TG}(\omega;r)\frac{\sin(k_m z)}{\sin(k_m L/2)} + \sum_{m=1}^{\infty} C_m\psi_m^{A}(\omega;r)\frac{\sinh(\kappa_m z)}{\sinh(\kappa_m L/2)}. \tag{33}$$

For $|z| > L/2$, Eq. (13) reduces to Laplace's equation, and thus, in this region, the mode potential can be expressed as a linear combination of vacuum solutions,

$$\delta\varphi_\omega(r,z) = \mathrm{sign}(z)\sum_{n=1}^{\infty} A_n J_0(\chi_{0n}r/R)e^{-\chi_{0n}(z-L/2)/R}. \tag{34}$$

Here, we have assumed that the mode potential is odd in z; the generalization to even modes is straightforward.

For the sake of numerical tractability, we must approximate Eqs. (33) and (34) by the partial series

$$\delta\varphi_\omega(r,z) = \sum_{m=1}^{N/2} B_m \psi_m^{TG}(\omega;r)\frac{\sin(k_m z)}{\sin(k_m L/2)} + \sum_{m=1}^{N/2} C_m \psi_m^{A}(\omega;r)\frac{\sinh(\kappa_m z)}{\sinh(\kappa_m L/2)} \tag{35}$$

and

$$\delta\varphi_\omega(r,z) = \mathrm{sign}(z)\times\sum_{m=1}^{N} A_m J_0(\chi_{0m} r/R) e^{-\chi_{0m}(z-L/2)/R}, \tag{36}$$

where N is some finite number of basis functions presumed to be sufficient to represent the mode to the desired degree of accuracy.

Note that the set of basis functions used here is not complete in the usual sense; we have only assumed that it is sufficient to represent a global solution to the mode equation with frequency ω. Expressing the global solution as a linear combination of local solutions in distinct domains has the advantage that convergence is much faster than would be the case if a more conventional basis was employed—for example, if the Fourier expansion $\delta\varphi_\omega = \sum_{m,n} A_{mn} J_0(\chi_{0m} r/R)\sin[(2n-1)z/L]$ was used in place of Eq. (35). Suppose that, in order to achieve some prescribed level of resolution of the mode, N^2 basis functions from the more standard basis are required; the same resolution can be achieved with just N basis functions of the type used here.

Taken together, the series (35) and (36) satisfy Eq. (13) everywhere inside the trap; all that remains is to find a set of coefficients, A_m, B_m, and C_m, and a frequency, ω, such that the resulting mode potential satisfies the required matching conditions at the boundary, $z = \pm L/2$. One such condition is that $\delta\varphi$ be continuous at $z = \pm L/2$. Thus, we evaluate Eqs. (35) and (36) at $z = \pm L/2$, equate the resulting expressions, multiply by $J_0(\chi_{0n} r/R)$, and integrate to obtain

$$\frac{R^2}{2}J_1^2(\chi_{0n})A_n = \sum_{m=1}^{N/2} B_m \int_0^R r dr J_0(\chi_{0n} r/R)\psi_m^{TG}(\omega;r) + \sum_{m=1}^{N/2} C_m \int_0^R r dr J_0(\chi_{0n} r/R)\psi_m^{A}(\omega;r). \tag{37}$$

The other matching condition is that the z-component of the electric displacement, $\delta D_z = [\omega_p^2(r,z)/\omega^2 - 1]\partial\delta\varphi/\partial z$, be continuous at $z = \pm L/2$. Accordingly, we equate the "inner" and "outer" expressions for δD_z resulting from Eqs. (35) and (36), respectively. An inner product with $\psi_m^{TG}(\omega;r)$ then yields

$$\frac{R^2}{2}k_m\cot(k_m L/2)B_m = \sum_{n=1}^{N} A_n(\chi_{0n}/R)\int_0^R r dr J_0(\chi_{0n} r/R)\times\psi_m^{TG}(\omega;r), \tag{38}$$

while an inner product with $\psi_m^{A}(\omega;r)$ yields

$$-\frac{R^2}{2}\kappa_m\coth(\kappa_m L/2)C_m = \sum_{n=1}^{N} A_n(\chi_{0n}/R)\int_0^R r dr J_0(\chi_{0n} r/R)\psi_m^{A}(\omega;r). \tag{39}$$

Note that we have employed the orthogonality relations (30) and (31) in obtaining Eqs. (38) and (39). Elimination of A_n in Eqs. (38) and (39) using Eq. (37) yields two sets of coupled equations for the amplitudes of the Trivelpiece-Gould and vacuum components, B_m and C_m,

$$k_m\cot(k_m L/2)B_m - \sum_{m'=1}^{N/2} B_{m'}\sum_{n=1}^{N}\frac{\chi_{0n}}{R}\times\frac{\int_0^R r dr J_0(\chi_{0n} r/R)\psi_{m'}^{TG}(\omega;r)}{R^2 J_1(\chi_{0n})/2}\frac{\int_0^R r dr J_0(\chi_{0n} r/R)\psi_{m}^{TG}(\omega;r)}{R^2 J_1(\chi_{0n})/2} - \sum_{m'=1}^{N/2} C_{m'}\sum_{n=1}^{N}\frac{\chi_{0n}}{R}\frac{\int_0^R r dr J_0(\chi_{0n} r/R)\psi_{m'}^{A}(\omega;r)}{R^2 J_1(\chi_{0n})/2}\times\frac{\int_0^R r dr J_0(\chi_{0n} r/R)\psi_{m}^{TG}(\omega;r)}{R^2 J_1(\chi_{0n})/2} = 0. \tag{40}$$

and

$$\kappa_m\coth(\kappa_m L/2)C_m + \sum_{m'=1}^{N/2} B_{m'}\sum_{n=1}^{N}\frac{\chi_{0n}}{R}\times\frac{\int_0^R r dr J_0(\chi_{0n} r/R)\psi_{m'}^{TG}(\omega;r)}{R^2 J_1(\chi_{0n})/2}\frac{\int_0^R r dr J_0(\chi_{0n} r/R)\psi_{m}^{A}(\omega;r)}{R^2 J_1(\chi_{0n})/2} + \sum_{m'=1}^{N/2} C_{m'}\sum_{n=1}^{N}\frac{\chi_{0n}}{R}\frac{\int_0^R r dr J_0(\chi_{0n} r/R)\psi_{m'}^{A}(\omega;r)}{R^2 J_1(\chi_{0n})/2}\times\frac{\int_0^R r dr J_0(\chi_{0n} r/R)\psi_{m}^{A}(\omega;r)}{R^2 J_1(\chi_{0n})/2} = 0. \tag{41}$$

Equations (40) and (41) specify N equations for N unknowns, which can be expressed in matrix notation as

$$\sum_{m'=1}^{N} M_{mm'}(\omega)x_{m'} \quad [\text{or } \mathbf{M}(\omega)\cdot\mathbf{x} = 0], \tag{42}$$

where $\mathbf{x} = (B_1, B_2, \ldots, B_{N/2}, C_1, C_2, \ldots, C_{N/2})$ and $\mathbf{M}(\omega)$ is a symmetric matrix with elements

$$M_{mm'}(\omega) = k_m\cot(k_m L/2)\delta_{mm'} - \sum_{n=1}^{N}\frac{\chi_{0n}}{R}\times\frac{\int_0^R r dr J_0(\chi_{0n} r/R)\psi_{m'}^{TG}(\omega;r)}{R^2 J_1(\chi_{0n})/2}\times\frac{\int_0^R r dr J_0(\chi_{0n} r/R)\psi_{m}^{TG}(\omega;r)}{R^2 J_1(\chi_{0n})/2} \tag{43}$$

for $m \leq N/2$ and $m' \leq N/2$,

$$M_{mm'}(\omega) = \kappa_m \coth(\kappa_m L/2)\delta_{mm'} - \sum_{n=1}^{N} \frac{\chi_{0n}}{R} \times \frac{\int_0^R r dr J_0(\chi_{0n} r/R)\psi^A_{m'}(\omega;r)}{R^2 J_1(\chi_{0n})/2} \times \frac{\int_0^R r dr J_0(\chi_{0n} r/R)\psi^A_{m}(\omega;r)}{R^2 J_1(\chi_{0n})/2} \quad (44)$$

for $N/2 < m \leq N$ and $N/2 < m' \leq N$, and

$$M_{mm'}(\omega) = -\sum_{n=1}^{N} \frac{\chi_{0n}}{R} \frac{\int_0^R r dr J_0(\chi_{0n} r/R)\psi^A_{m'}(\omega;r)}{R^2 J_1(\chi_{0n})/2} \times \frac{\int_0^R r dr J_0(\chi_{0n} r/R)\psi^{TG}_{m}(\omega;r)}{R^2 J_1(\chi_{0n})/2} \quad (45)$$

for $m \leq N/2$ and $N/2 < m' \leq N$. Equation (42) constitutes a generalized eigenvalue problem; each matrix element depends on the unknown mode frequency, ω through the functions $\psi^{TG}_m(\omega;r)$ and $\psi^A_m(\omega;r)$ and the wavenumbers $k_m = k_m(\omega)$ and $\kappa_m = \kappa_m(\omega)$.

A. Analytic solution for $a = R$

In order to better understand the matrix equation (42), it is instructive to consider the simple case in which the plasma extends to the trap wall—that is, $a = R$. In this case, there are no annular solutions, so the matrix $\mathbf{M}$ is given entirely by Eq. (43). Furthermore, the TG solutions have the same radial dependence as the vacuum solutions,

$$\psi^{TG}_m(\omega;r) = \frac{k_m^2(\omega)}{(\chi_{0m}/R)^2} \frac{J_0(\chi_{0m} r/R)}{J_1(\chi_{0m})} \quad (46)$$

[the normalization follows from Eq. (30)]. Consequently, the second term on the right-hand side of Eq. (43) is zero unless $m = m'$, implying that a given TG wave reflects entirely back into itself at $z = \pm L/2$. In other words, the matrix $\mathbf{M}$ is diagonal, and Eq. (46) takes the simple form

$$[k_m \cot(k_m L/2) - k_m^2 R/\chi_{0m}]B_m = 0. \quad (47)$$

Thus, when the plasma extends to the trap wall, the modes are just standing TG waves with radial dependence given by Eq. (46) and axial wavenumber quantized according to the condition that the diagonal matrix element equal zero,

$$\cot(k_m L/2) - k_m R/\chi_{0m} = 0. \quad (48)$$

For a long plasma, it follows that for radial modenumber m, the allowed axial wavenumbers are given by $k_{mn} = (2n-1)\pi/L - \delta k_{mn}$, where n is an integer and δk_{mn} is a correction of order R/L^2. Inserting this expression in Eq. (48) and expanding the cotangent term, one finds that to first order in R/L^2, $\delta k_{mn} \cong (2n-1)2\pi R/(\chi_{0m} L^2)$.

B. Numerical solution for $a < R$

When the plasma does not extend to the trap wall, the radialdependence of the TG waves no longer matches that of the vacuum solutions. Consequently, at $z = \pm L/2$, an incident TG wave reflects partially back into itself and partially into other TG waves. It follows that each mode must be a mixture of multiple component waves. From a cursory analysis of the matrix $\mathbf{M}$, one can guess which waves should appear prominently in the admixture for a mode with frequency ω. According to the normalization condition (30), the second term on the right-hand side of Eq. (43)—and thus any off-diagonal matrix element—is of order R/L^2 or smaller.[11] In contrast, the first term on the right-hand side of Eq. (43), which appears only on the diagonal of the matrix, can be any size, diverging as $k_m(\omega)L/2$ approaches any multiple of π, and vanishing as $k_m(\omega)L/2$ approaches any odd multiple of $\pi/2$. If the wavenumber $k_m(\omega)$ is such that $k_m \cot(k_m L/2)| \gg R/L^2$, the mth diagonal element will be large, and one can see that the amplitude of the mth wave must then be small in order for Eq. (42) to be satisfied. Conversely, the amplitude of the mth wave may be large only if the mth diagonal element is small compared to R/L^2; as in the previous example, this occurs for wavenumbers $k_m(\omega) = (2n-1)\pi/L - \delta k_m(\omega)$, where n is an integer and $\delta k_m(\omega)$ is a correction of order R/L^2. For a given mode frequency, there can be many such waves, and these waves will give the dominant contribution to the admixture for that mode.

The heuristic argument outlined in the preceding paragraph is a revised version of an argument introduced by Prasad and O'Neil.[11] These authors derived a generalized version of Eq. (10) for a mode with azimuthal dependence and carried out a perturbative solution based on the smallness of the off-diagonal matrix elements. However, a tacit assumption underlying the perturbation theory is that only one of the diagonal elements of the matrix is small compared to the off-diagonal elements in its row, and this assumption is unjustified.

We proceed by evaluating the matrix $\mathbf{M}(\omega)$ on a grid in ω-space and calculating the determinant at each point on this grid. We search for values of ω for which $\mathrm{Det}[\mathbf{M}(\omega)] = 0$, at these values, the null-vector, $\mathbf{x}$, gives a solution to Eq. (42). As expected, the contribution to each solution is greatest from wavenumbers $k_m(\omega) \cong (2n-1)\pi/L$. However, as the number of basis functions, N, is increased, increasingly short-wavelength waves enter the admixture for each solution with significant amplitude, and this trend continues to the limit of our computational capability. The lack of convergence should not be surprising. The off-diagonal matrix elements fall off only as m^{-1} and are non-negligible even for large m; thus, for arbitrarily large m, the mth diagonal matrix element can still be smaller than the off-diagonal elements in the mth row, provided that the wavenumber k_m is close enough to $(2n-1)\pi/L$, where n is an integer.

An exemplary solution is plotted in Fig. 5—with various numbers of basis functions retained—as an illustration of the appearance of increasingly large wavenumbers in each solution. In Fig. 5(a), only four TG waves are retained, and the dominant term in the admixture comes from the first TG

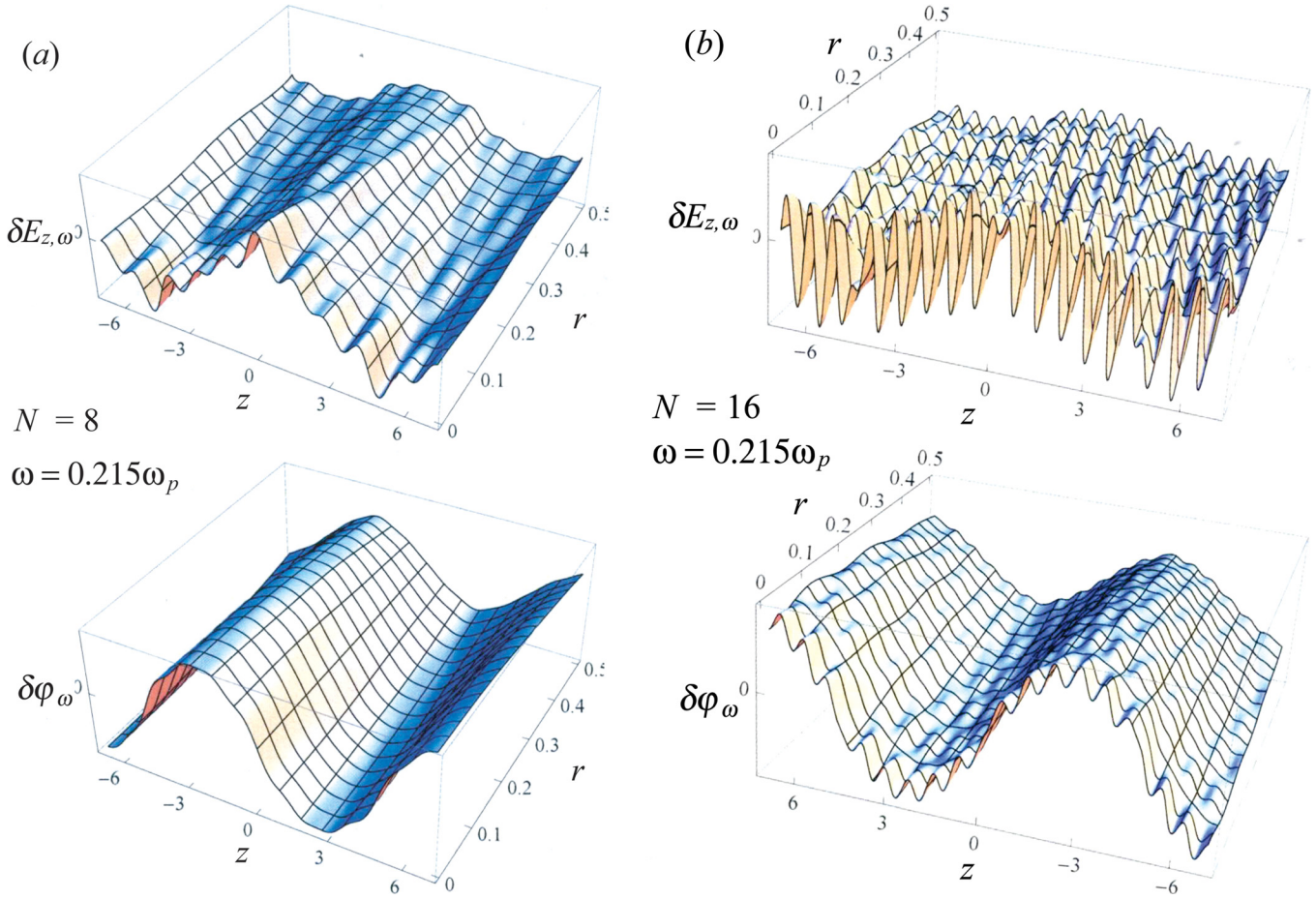

FIG. 5. (Color online) The axial electric field, $\delta E_{z,\omega}$, and potential, $\delta\varphi_\omega$, corresponding to a solution of the matrix equation (42) obtained by retaining 8 terms (a) and 16 terms (b) in the series (35) and (36). The plasma has length $L = 14.0$ and radius $a = 0.5$, and the trap has radius $R = 1.0$. As the number of basis functions is increased, the solution involves increasingly large wavenumbers.

wave, which has wavenumber $k_1(\omega) \cong 3\pi/L - 6.94(R/L^2)$, where ω is the frequency of the solution. In Fig. 5(b), eight waves are retained, and now the seventh wave, which has wavelength $k_7(\omega) \cong 39\pi/L - 2.45(R/L^2)$, enters the admixture with amplitude comparable to that of the first wave. With more waves retained, the solution incurs significant contributions from even shorter wavelengths.

V. MODES OF A PLASMA COLUMN WITH SPHEROIDAL END-SHAPE

There is a reason to suspect that the appearance of increasingly short wavelengths in each of the solutions obtained in Sec. IV stems from the crude approximation of the plasma shape as a cylinder with perfectly flat ends and hence sharp edges. The mode structure is determined by the coupling between TG waves reflecting at the ends of the plasma cylinder, and this coupling must be affected by the end-shape. In this section, we generalize the method of Sec. IV and look for modes of a plasma cylinder with spheroidal end-shape. In this case, the plasma boundary is given by $r = a$ for $|z| < L/2$ and by $[(z - L/2)/(\Delta L_0/2)]^2 + (r/a)^2 = 1$ for $|z| > L/2$, where ΔL_0 is the combined length of the two spheroidal end caps. Note that this plasma boundary has no sharp edges. For long cylindrical plasmas satisfying the ordering $L \gg R \sim a$, the curvature of the ends of the plasma cylinder in equilibrium is typically of order $1/a$, so we will consider end-shapes with ΔL_0 of order a.[3]

Following the procedure of Sec. IV, we divide the space inside the trap into regions with distinct solution sets, as depicted in Fig. 3(b). The surface that separates these regions is given by $z = [L + \Delta L(r)]/2$, where

$$\frac{\Delta L(r)}{2} = \begin{cases} (\Delta L_0/2)\sqrt{1-(r/a)^2} & r < a \\ 0 & a < r < R \end{cases} \tag{49}$$

is the deviation from the flat matching surface taken in Sec. VI. We express the mode potential as the series (35) and (36) in the appropriate domains. Again, the matching conditions on $\delta\varphi$ and $\delta\mathbf{D} = [\omega_p^2(r,z)/\omega^2 - 1](\partial\delta\varphi/\partial z)\hat{\mathbf{z}} - (\partial\delta\varphi/\partial r)\hat{\mathbf{r}}$ yield coupled equations for the coefficients B_n and C_n. The continuity of $\delta\varphi$ gives

$$\sum_{n=1}^{N} A_n J_0(\chi_{0n} r/R) e^{-\chi_{0n}\Delta L(r)(2R)} = \sum_{m=1}^{N/2} B_m \psi_m^{TG}(\omega;r) \frac{\sin\{k_m(\omega)[L+\Delta L(r)]/2\}}{\sin\{k_m(\omega)L/2\}} + \sum_{m=1}^{N/2} C_m \psi_m^{A}(\omega;r) \frac{\sinh\{\kappa_m(\omega)[L+\Delta L(r)]/2\}}{\sinh\{\kappa_m(\omega)L/2\}}, \tag{50}$$

while the continuity of $\delta\mathbf{D}\cdot\hat{\mathbf{n}}$ gives

$$\sum_{n=1}^{N}A_n(\chi_{0n}/R)e^{-\chi_{0n}\Delta L(r)/(2R)}[n_z(r)J_0(\chi_{0n}r/R)+n_r(r)J_1(\chi_{0n}r/R)]$$
$$=-\sum_{m=1}^{N/2}B_m\left[n_r(r)\frac{d\psi_m^{TG}(\omega;r)\sin\{k_m(\omega)[L+\Delta L(r)]/2\}}{dr\qquad\sin\{k_m(\omega)L/2\}}\right.$$
$$\left.+n_z(r)\varepsilon(\omega,r)k_m(\omega)\psi_m^{TG}(\omega;r)\frac{\cos\{k_m(\omega)[L+\Delta L(r)]/2\}}{\sin\{k_m(\omega)L/2\}}\right]$$
$$-\sum_{m=1}^{N/2}C_m\left[n_r(r)\frac{d\psi_m^{A}(\omega;r)\sinh\{\kappa_m(\omega)[L+\Delta L(r)]/2\}}{dr\qquad\sinh\{\kappa_m(\omega)L/2\}}\right.$$
$$\left.+n_z(r)\varepsilon(\omega,r)\kappa_m(\omega)\psi_m^{A}(\omega;r)\frac{\cosh\{\kappa_m(\omega)[L+\Delta L(r)]/2\}}{\sinh\{\kappa_m(\omega)L/2\}}\right], \tag{51}$$

where $n_r(r)$ and $n_z(r)$ are the radial and axial components of the unit vector $\hat{\mathbf{n}}$ that is normal to the matching surface.

The analysis of Sec. IV relies on the orthogonality properties of the Bessel functions and the functions $\psi_m^{TG}(\omega;r)$ and $\psi_m^{A}(\omega;r)$, however, this approach fails here because the curvature of the plasma boundary introduces additional r-dependence. Instead, we discretize the radial coordinate, taking P points, $\{r_1, r_2,\ldots, r_P\}$, and evaluate Eqs. (50) and (51) on this grid, obtaining two sets of coupled equations,

$$\sum_{n=1}^{N}A_nJ_0(\chi_{0n}r_p/R)e^{-\chi_{0n}\Delta L(r_p)/(2R)}$$
$$=\sum_{m=1}^{N/2}B_m\psi_m^{TG}(\omega;r_p)\frac{\sin\{k_m(\omega)[L+\Delta L(r_p)]/2\}}{\sin\{k_m(\omega)L/2\}}$$
$$+\sum_{m=1}^{N/2}C_m\psi_m^{A}(\omega;r_p)\frac{\sinh\{\kappa_m(\omega)[L+\Delta L(r_p)]/2\}}{\sinh\{\kappa_m(\omega)L/2\}} \tag{52}$$

and

$$\sum_{n=1}^{N}A_n(\chi_{0n}/R)e^{-\chi_{0n}\Delta L(r)/(2R)}$$
$$\times[n_z(r_p)J_0(\chi_{0n}r_p/R)+n_r(r_p)J_1(\chi_{0n}r_p/R)]$$
$$=-\sum_{m=1}^{N/2}B_m\left[n_r(r_p)\left.\frac{d\psi_m^{TG}(\omega;r)}{dr}\right|_{r=r_p}\right.$$
$$\times\frac{\sin\{k_m(\omega)[L+\Delta L(r_p)]/2\}}{\sin\{k_m(\omega)L/2\}}+n_z(r_p)\varepsilon(\omega,r_p)k_m(\omega)$$
$$\left.\times\psi_m^{TG}(\omega;r_p)\frac{\cos\{k_m(\omega)[L+\Delta L(r_p)]/2\}}{\sin\{k_m(\omega)L/2\}}\right]$$
$$-\sum_{m=1}^{N/2}C_m\left[n_r(r_p)\left.\frac{d\psi_m^{A}(\omega;r)}{dr}\right|_{r=r_p}\right.$$
$$\times\frac{\sinh\{\kappa_m(\omega)[L+\Delta L(r_p)]/2\}}{\sinh\{\kappa_m(\omega)L/2\}}+n_z(r_p)\varepsilon(\omega,r_p)\kappa_m(\omega)$$
$$\left.\times\psi_m^{A}(\omega;r_p)\frac{\cosh\{\kappa_m(\omega)[L+\Delta L(r_p)]/2\}}{\sinh\{\kappa_m(\omega)L/2\}}\right]. \tag{53}$$

Equations (52) and (53) comprise a system of $2P$ equations for $2N$ unknowns and can be expressed as a single matrix equation,

$$\sum_{n=1}^{2N}M'_{pn}(\omega)x'_n=0\quad[\text{or }\mathbf{M}'(\omega)\cdot\mathbf{x}'=0], \tag{54}$$

where $\mathbf{x}'=(A_1,A_2,\ldots,A_N,B_1,B_2,\ldots,B_{N/2},C_1,C_2,\ldots,C_{N/2})$ and $\mathbf{M}'(\omega)$ is a $2P\times 2N$ matrix; the primes are a reminder that the matrix $\mathbf{M}'$ and the vector $\mathbf{x}'$ are distinct from $\mathbf{M}$ and $\mathbf{x}$ as defined in Sec. IV.

In order for every basis function to be well-resolved on the radial grid, we take $P\gg N$, and thus, Eq. (54) becomes an over-determined system of equations that cannot be satisfied exactly. Thus, we seek a nonzero vector $\mathbf{x}'$ and frequency ω that together minimize the mean squared mismatch at the boundary, $\Delta(\omega,\mathbf{x}')$, defined as

$$\Delta(\omega,\mathbf{x}')\equiv\frac{1}{P}[\mathbf{M}'(\omega)\cdot\mathbf{x}']^2. \tag{55}$$

We exclude the trivial solution, $\mathbf{x}'=0$, by imposing a normalization constraint. We observe that a variety of different normalization constraints lead to the same solutions. A simple choice is the following:

$$[\mathbf{S}(\omega)\cdot\mathbf{x}']^2=1, \tag{56}$$

where

$$S_{nn'}(\omega)=\frac{k_n(\omega)\delta_{nn'}}{\sin[k_n(\omega)L/2]}, \tag{57}$$

for $n\le N/2$ and $S_{nn'}=0$ otherwise. This constraint simply requires that the squared amplitudes of all Trivelpiece-Gould components making up the mode electric field sum to one.

For fixed ω, the minima of $\Delta(\omega,\mathbf{x}')$ under this normalization constraint are given by the condition

$$\delta\Big([\mathbf{M}'(\omega)\cdot\mathbf{x}']^2-\lambda\{[\mathbf{S}(\omega)\cdot\mathbf{x}']^2-1\}\Big)=0, \tag{58}$$

where λ is a Lagrange multiplier and the variation is taken with respect to $\mathbf{x}'$. Carrying out the variation yields

$$\mathbf{M}'^T(\omega)\cdot\mathbf{M}'(\omega)\cdot\mathbf{x}'=\lambda\mathbf{S}^T(\omega)\cdot\mathrm{S}(\omega)\cdot\mathbf{x}', \tag{59}$$

where the superscript T denotes the transpose. In other words, for fixed ω the local minima of $\Delta(\omega,\mathbf{x}')$ are given by the "generalized eigenvectors" of the matrix $\mathbf{M}'^T(\omega)\cdot\mathbf{M}'(\omega)$ with respect to the matrix $\mathbf{S}^T(\omega)\cdot\mathbf{S}(\omega)$. The global minimum (on the surface of constraint) is given by the eigenvector with the smallest eigenvalue; all eigenvalues are positive since both $\mathbf{M}'^T(\omega)\cdot\mathbf{M}'(\omega)$ and $\mathbf{S}^T(\omega)\cdot\mathbf{S}(\omega)$ are positive-definite.

To find a mode frequency, we therefore evaluate the matrices $\mathbf{M}'^T(\omega)\cdot\mathbf{M}'(\omega)$ and $\mathbf{S}^T(\omega)\cdot\mathbf{S}(\omega)$ on a grid in ω and determine the smallest eigenvalue, $\lambda_{\min}(\omega)$, at each grid point. For $N\gg 1$, the function $\lambda_{\min}(\omega)$ typically has many local minima. As N and P are increased, some of these minima approach zero (as does the corresponding mismatch), and the value of ω, where such a minimum occurs, gives the frequency of a mode. The mode potential is given by the eigenvector, $\mathbf{x}'$, corresponding to $\lambda_{\min}(\omega)$ at the mode frequency. The procedure is illustrated in Fig. 6.

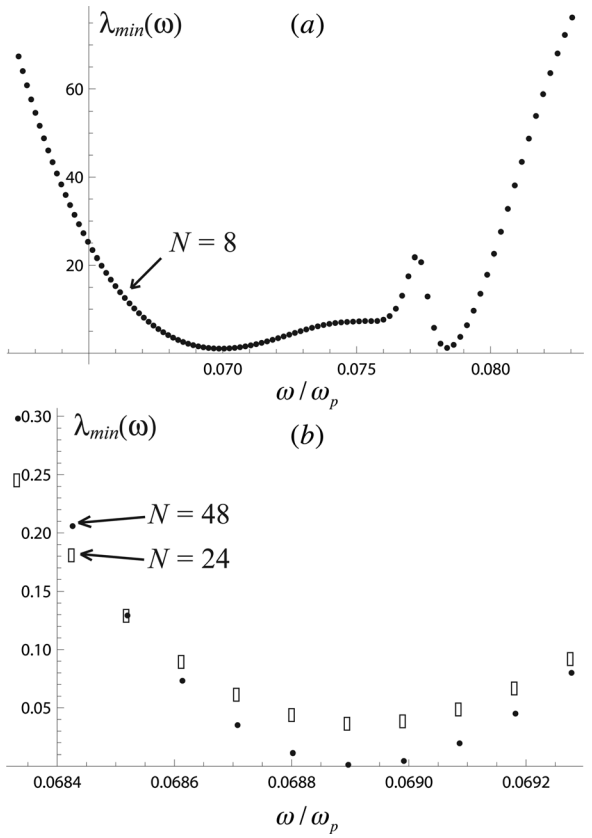

FIG. 6. (a) Evaluation of the function $\lambda_{\min}(\omega)$ on a grid in ω for $N = 8$ basis functions. The local minima near $\omega = 0.070\omega_p$ and $\omega = 0.078\omega_p$ indicate the frequencies of two low-order modes. (b) Evaluation of the function $\lambda_{\min}(\omega)$ on a finer grid in ω for $N = 24$ (open rectangles) and $N = 48$ (solid circles) basis functions.

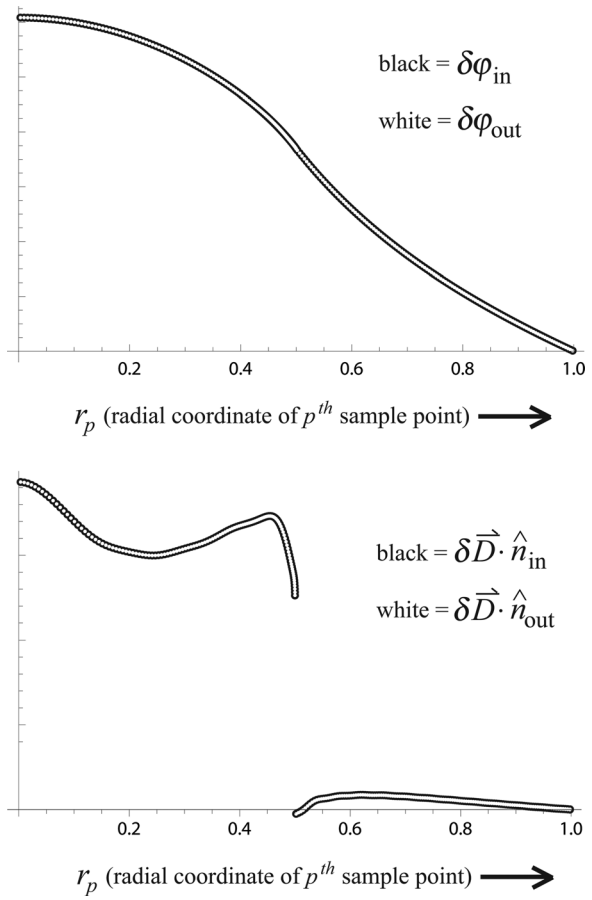

FIG. 7. An example of the matching of the mode potential, $\delta\varphi_\omega$ and normal component of the electric displacement, $\delta\mathbf{D}_\omega \cdot \hat{\mathbf{n}}$, at the sample points along the matching surface. Each black circle gives the value of the right-hand side of Eq. (52) or (53) at these sample points; that is, the value of the electric potential or normal component of the electric displacement as the sample point is approached from inside. Each white circle gives the value of the left-hand side of Eq. (52) or (53) at these sample points; that is, the value of the electric potential or normal component of the electric displacement as the sample point is approached from outside. Note that the white circles lie on top of the black circles. Here, $N = 48$ and $P = 240$ The spatial dependence of this mode is displayed in Fig. 8(a).

In practice, when only a few terms are retained in the series (35) and (36) and the corresponding function $\lambda_{\min}(\omega)$ is plotted, one observes relatively few local minima, and the location of each minimum gives a rough indication of the frequency of a mode comprised mostly of long-wavelength waves [Fig. 6(a)]. Using this information, one can then keep many more terms in the series and plot the corresponding function $\lambda_{\min}(\omega)$ over a much smaller frequency interval about one of these minima [Fig. 6(b)]. Of course, this strategy only works for the relatively smooth modes comprised mostly of long-wavelength waves, but these are typically the most relevant modes in an experiment. An example of the matching of the potential and electric displacement at the sample points along the matching surface is shown in Fig. 7; in this example, the numbers of basis functions and sample points retained are $N = 48$ and $P = 240$, respectively. Note that two sets of points in Fig. 7 lie on top of each other, indicating good matching.

Several exemplary solutions are plotted in Fig. 8. We observe that strong mixing occurs only amongst waves with axial wavelengths larger than the variation in plasma length, ΔL_0, and in particular for wavenumbers $k_m \cong (2n-1)\pi/L$, where n is an integer. For example, Fig. 8(a) shows a mode that is mostly a mixture of the $m = 1$ and $m = 2$ waves having wavenumbers $k_1 \cong \pi/L$ and $k_2 \cong 3\pi/L$. [Recall that the wavenumbers $k_m = k_m(\omega)$ of the component waves are determined by Eq. (26) and the frequency of the mode, ω.]

Waves with shorter axial wavelengths are less strongly mixed but tend to add constructively to create fine-scale cone-like structures in the mode along resonance cones with slope $dz/dr = \pm(\omega_p^2/\omega^2 - 1)^{1/2}$. The modes shown in Figs. 8(b) and 8(c) exhibit these cone-like features.

It should be noted that Jennings *et al*. also find solutions to the mode equation that do not resemble any single Trivelpiece-Gould wave.[12] In addition, the authors note that according to Eq. (14), very different waveforms can have similar frequencies. However, Jennings *et al*. conclude that the more complicated solutions are not real modes, but the result of miscalculation by the numerical algorithm. Presumably, this work was motivated by experiments involving warm plasmas, in which Landau damping rates consistent with the single-wave approximation had been observed, so the complicated solutions were not investigated further.

By choosing $L \ll \Delta L_0$ and $a \ll R$, we approach the limit where Dubin's theory for modes of a spheroidal plasma should apply.[7] An example of a solution obtained in this limit is depicted in Fig. 9(a); Fig. 9(b) depicts the

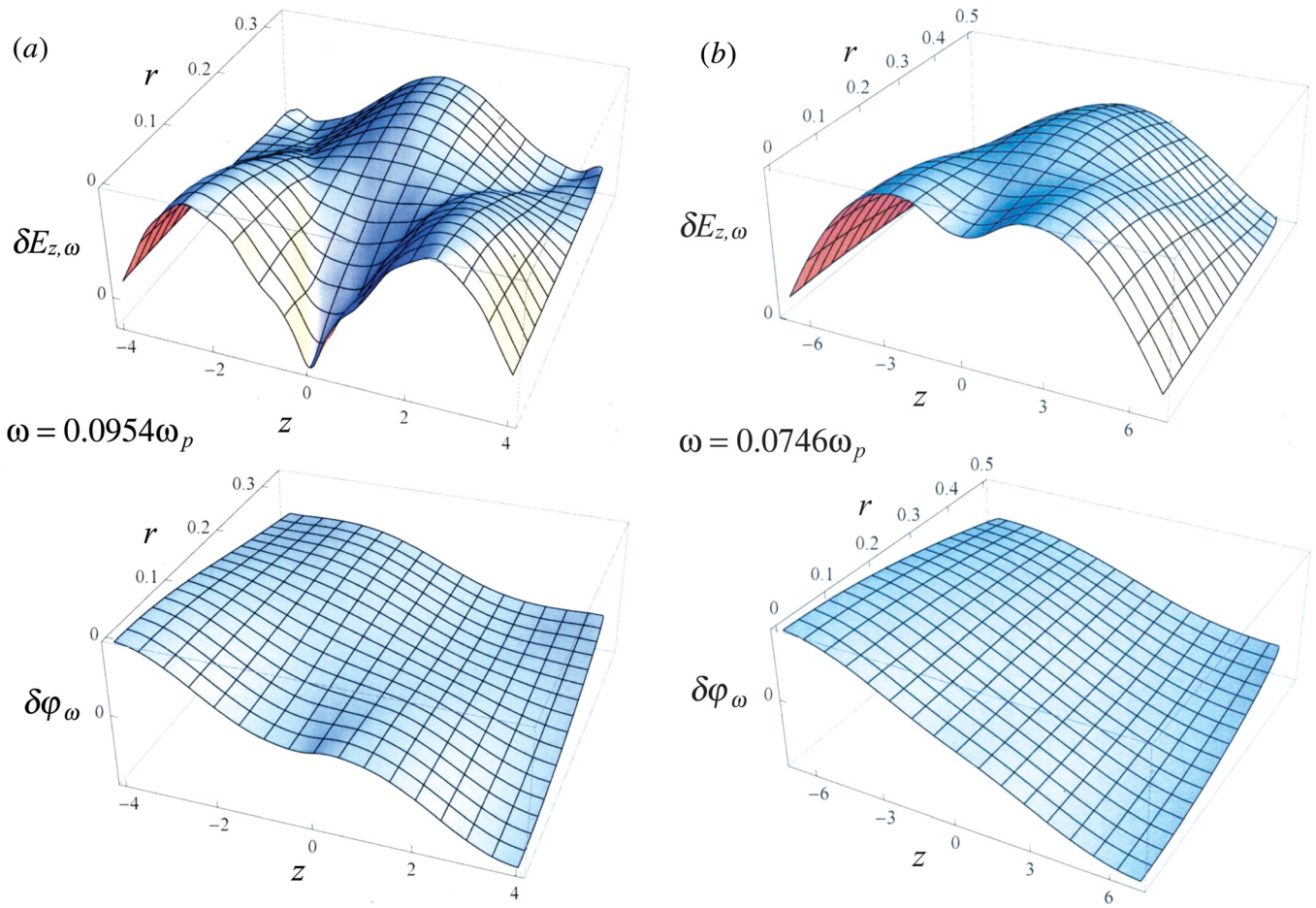

FIG. 8. (Color online) (a) The axial electric field, $\delta E_{z,\omega}$, and potential, $\delta\varphi_\omega$, of a normal mode of a plasma with length $L+\Delta L_0 = 8.0$, radius $a = 0.33$, and end-shape $\Delta L_0 = a$; note the strong mixing of the $m = 1$ and $m = 2$ components. (b) and (c) Two normal modes of a plasma cylinder with length $L+\Delta L_0 = 14.0$ radius $a = 0.5$, and end-shape given by Eq. (42) with $\Delta L_0 = 2a$. (d) and (e) Two normal modes of a plasma cylinder with length $L+\Delta L_0 = 14.0$ radius $a = 0.5$, and end shape given by $\Delta L_0 = a$. In (a)-(e), the domain of each plot is the interior of the plasma, and the radius of the trap is $R = 1.0$.

corresponding Dubin mode for comparison. It should be mentioned that the convergence of the solutions for spheroidal plasmas is slower than for long, cylindrical plasmas; that is, for a given number of basis functions, the mismatch at the sample points $\{r_1, r_2, \ldots, r_P\}$ tends to be larger. While Fig. 9(a) represents the limit of our computational capabilities, we expect that if many more basis functions could be retained, the mismatch would tend to zero without significant change in the appearance of the mode potential. However, the high-k features appearing in the electric field could be artifacts of the incomplete convergence.

VI. MODES OF A NEARLY SPHEROIDAL PLASMA

Thus far we have used numerical solutions to investigate the effect of degeneracy on the modes of a cold cylindrical plasma with rounded ends. In this section, we exploit the fact that analytic solutions are known for the modes of a cold, magnetized, uniform-density plasma of spheroidal shape (the Dubin modes) and use perturbation theory to investigate the mixing of low-order, nearly degenerate Dubin modes.

A cold non-neutral plasma, which resides in a quadratic trap potential and has dimensions small compared to the distance to the electrodes, evolves to thermal equilibrium shape that is a uniform density spheroid.[2,6] Here, we use perturbation theory to understand how small deviations of the trap potential from quadratic change the spheroidal shape and mix nearly degenerate low-order Dubin modes. We work out the general form of the mode-mode coupling and examine the mixing of the axial center-of-mass (CM) mode with higher-order modes as an example.

In the axial CM mode, the spheroid oscillates as a whole along the magnetic axis and with each particle in the plasma moving in the axial direction according to

$$\delta z(t) = \varepsilon\cos(\omega_z t), \tag{60}$$

where ε is a constant amplitude and ω_z is the axial trap frequency, determined by the harmonic external trap potential $q\varphi_{ext}(r,z) = (1/2)m\omega_z^2(z^2 - r^2/2)$. Here, we consider a perturbation $\Delta\varphi(\mathbf{r})$ to the external potential,

$$q\varphi_{ext}(r,\theta,z) = \frac{1}{2}m\omega_z^2\left(z^2 - \frac{1}{2}r^2\right) + q\Delta\varphi(r,\theta,z). \tag{61}$$

For the CM mode, the resulting frequency change (in the absence of degeneracy) can be worked out with a fairly simple argument. For each particle in the plasma, the axial equation of motion is

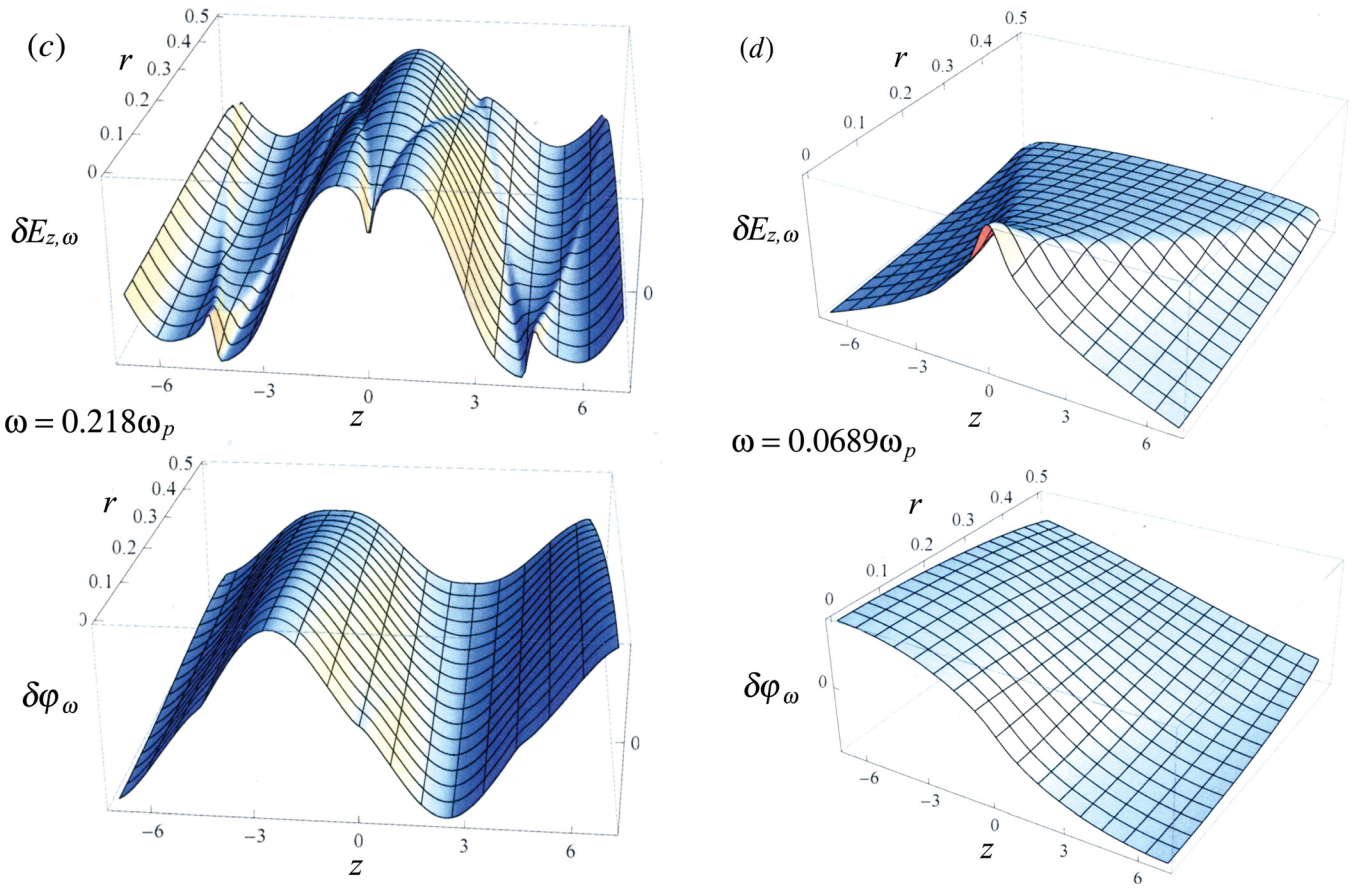

FIG. 8. (*Continued*)

$$\frac{d^2 z_i}{dt^2} = -\omega_z^2 z_i + \sum_{j\neq i} \frac{4\pi q^2}{m} \frac{\partial G(\mathbf{r}_i, \mathbf{r}_j)}{\partial z_i} - \frac{q}{m} \frac{\partial \Delta\varphi(\mathbf{r}_i)}{\partial z_i}, \quad (62)$$

where G is the Green's function satisfying $\nabla^2 G = \delta(\mathbf{r}_i - \mathbf{r}_j)$. Assuming that G has axial translational symmetry, so that it depends on z_i and z_j only through the combination $z_i - z_j$, we sum over the N particles to obtain expressions involving the center-of-mass position, Z,

$$\frac{d^2 Z}{dt^2} = -\omega_z^2 Z - \frac{q}{Nm} \sum_{i=1}^{N} \frac{\partial \Delta\varphi(\mathbf{r}_i)}{\partial z_i}. \quad (63)$$

If we now assume that the mode in question causes positions to vary according to $\mathbf{r}_i = \mathbf{r}_{i0} + \varepsilon \cos(\omega t)\hat{\mathbf{z}}$, we can use this expression in Eq. (63) to obtain

$$\omega^2 = \omega_z^2 + \frac{q}{Nm} \sum_{i=1}^{N} \frac{\partial^2 \Delta\varphi(\mathbf{r}_{i0})}{\partial^2 z_{i0}}. \quad (64)$$

Furthermore, since $\Delta\varphi$ is already small, we can neglect the shape change of the equilibrium and sum over equilibrium positions in a spheroid. For example, if

$$q\Delta\varphi = \frac{1}{2} m\omega_z^2 \sum_{n=3}^{\infty} \beta_n \frac{r^n}{R^{n-2}} P_n(\cos\theta) \quad (65)$$

(a spherical harmonic expansion, with R the distance to the trap electrodes), then Eq. (64) implies

$$\omega^2 = \omega_z^2 \left[1 + \frac{6}{5}\beta_4 \frac{(b^2 - a^2)}{R^2} + \frac{9}{7}\beta_6 \frac{(b^2 - a^2)^2}{R^4} + \cdots \right], \quad (66)$$

where $2a$ and $2b$ are, respectively, the diameter and length of the plasma spheroid.

This simple result provides a useful check for the following more general results. However, in particular, it neglects degeneracies between the CM mode and other modes. There are many such degenerate modes, each occurring when the plasma spheroid takes on a particular shape. A list of some of these modes is provided in Table I.[15] The mode numbers l and m refer to the spheroidal harmonic of the given mode potential,[7] and the parameter $\alpha \equiv b/a$ gives the plasma shape for which degeneracy with the CM mode occurs.

We now turn to the affect of perturbations on the mode eigenfunction (which must be determined using the above approach), including the effect of degeneracies, for general spheroidal normal modes. To do so, we employ the integral operator formalism introduced in Sec. II [Eq. (19)], where the normal modes of the axial electric field $\delta E_{z,\omega}(\mathbf{r})$ obey the eigenvalue equation

$$\omega^2 \delta E_{z,\omega}(\mathbf{r}) = -\int d^3\mathbf{r}' \omega_p^2(\mathbf{r}') \frac{\partial G(\mathbf{r}, \mathbf{r}')}{\partial z \partial z'} \delta E_{z,\omega}(\mathbf{r}'). \quad (67)$$

As discussed previously, the integral operator appearing on the right-hand-side is Hermitian with respect to the inner product $(f_1, f_2) \equiv \int d^3\mathbf{r} \omega_p^2(\mathbf{r}) f_1 f_2$, so that its eigenfunctions

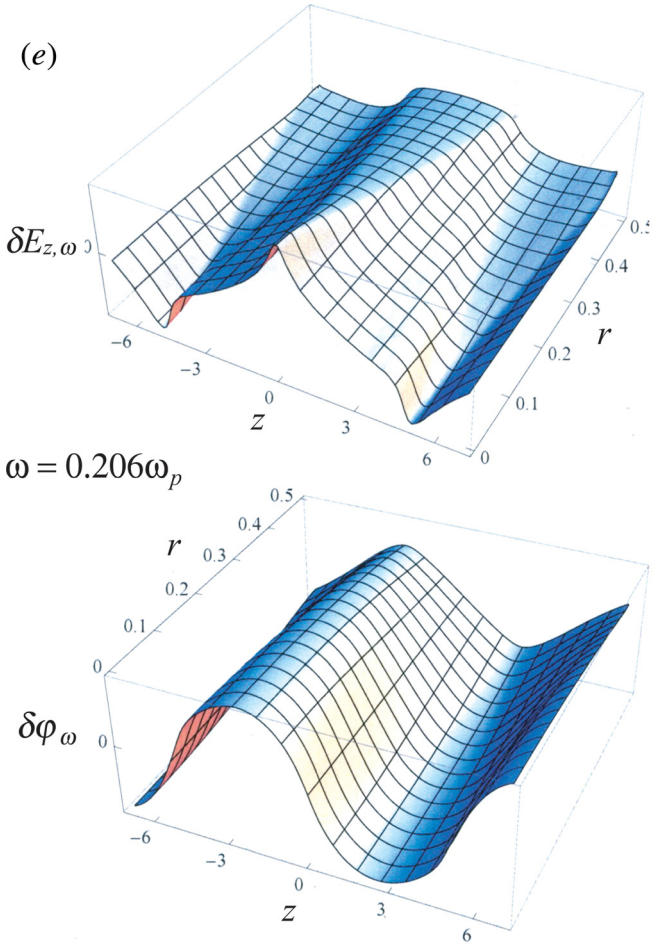

FIG. 8. (*Continued*)

form a complete orthogonal basis with respect to this inner product. However, as this is an integral operator, these eigenfunctions are not necessarily continuous functions. In fact, for a cold plasma with a sharp boundary, $\delta E_{z,\omega}(\mathbf{r})$ is discontinuous across this boundary. Since the perturbed external potential changes the shape of this boundary, the following perturbation theory is somewhat novel in form.

In the cold-fluid limit considered here, the perturbed potential $\Delta\varphi(\mathbf{r})$ causes a shape change to the plasma volume, V as shown in Fig. 10. The volume integral in Eq. (67) must be carried out over this volume. In order to apply perturbation theory, we inscribe a spheroid with volume V_0 inside V (see Fig. 10). The volume difference $\Delta V = V - V_0$ is assumed to be small. We then break the integral in Eq. (67) into integrals over V_0 and over ΔV,

$$\omega^2\delta E_{z,\omega}(\mathbf{r}) = -\int_{V_0} d^3\mathbf{r}'\omega_p^2\frac{\partial G(\mathbf{r},\mathbf{r}')}{\partial z\partial z'}\delta E_{z,\omega}(\mathbf{r}') - \int_{V_0} d^3\mathbf{r}'\omega_p^2\frac{\partial G(\mathbf{r},\mathbf{r}')}{\partial z\partial z'}\delta E_{z,\omega}(\mathbf{r}'). \quad (68)$$

We treat the second integral as a small perturbation. To do so, we expand $\delta E_{z,\omega}(\mathbf{r})$ in the eigenfunctions of the first integral operator for the spheroid V_0, with the following proviso. As previously noted, the eigenfunctions have distinct forms inside and outside the spheroid, which we refer to, respectively, as $\psi_n^{in}(\mathbf{r})$ and $\psi_n^{out}(\mathbf{r})$ (where $n = 1,\ldots,\infty$). We choose to represent $\delta E_{z,\omega}(\mathbf{r})$ only in terms of the inner eigenfunctions $\psi_n^{in}(\mathbf{r})$, extending their functional forms beyond V_0 into ΔV. These eigenfunctions have the form $e^{im\theta}f(r,z)$, where f is a finite polynomial in r and z; we assume (without proof) that such polynomials form a complete set for perturbations in the region ΔV. Thus, we write

$$\delta E_{z,\omega}(\mathbf{r}) = \sum_{n=1}^{M} a_n\psi_n^{in} + \sum_{m=M+1}^{\infty}\varepsilon_n\psi_n^{in}, \quad (69)$$

where the coefficients a_n are of order unity and $|\varepsilon_n| \ll 1$. For $M = 1$, we will obtain results for nondegenerate perturbation theory, and for $M > 1$ we will obtain results where M modes are nearly degenerate.

Substituting Eq. (69) into Eq. (68) and dropping small terms yields

$$\omega^2\left(\sum_{n=1}^{M} a_n\psi_n^{in} + \sum_{n=M+1}^{\infty}\varepsilon_n\psi_n^{in}\right) = \sum_{n=1}^{M}\omega_n^2 a_n\psi_n^{in} + \sum_{n=M+1}^{\infty}\omega_n^2\varepsilon_n\psi_n^{in} - \omega_p^2\sum_{n=1}^{M} a_n\int_{\Delta V} d^3\mathbf{r}'\frac{\partial^2 G}{\partial z\partial z'}\psi_n^{in}(\mathbf{r}'), \quad (70)$$

where the spheroidal mode frequencies ω_n are eigenvalues obtained from the equation

$$\omega_n^2\psi_n(\mathbf{r}) = -\omega_p^2\int_{V_0} d^3\mathbf{r}'\frac{\partial G}{\partial z\partial z'}\psi_n(r'). \quad (71)$$

Note that solutions of this integral equation yield $\psi_n^{in}(\mathbf{r})$ for $\mathbf{r} \in V_0$ and $\psi_n^{out}(\mathbf{r})$ for $\mathbf{r} \notin V_0$. If we now take an inner product of Eq. (70) with respect to the M ψ_n^{in} functions over volume V_0 and use their orthogonality, we obtain M homogeneous equations for the coefficients $a_1,\ldots,a_M$:

$$(\omega^2 - \omega_m^2)a_m = -\omega_p^2\sum_{n=1}^{M} a_n\frac{\int_{V_0} d^3\mathbf{r}\psi_m^{in*}(\mathbf{r})\int_{\Delta V} d^3\mathbf{r}'\frac{\partial G}{\partial z\partial z'}\psi_m^{in}(\mathbf{r}')}{\int_{V_0} d^3\mathbf{r}|\psi_m^{in}(\mathbf{r})|^2} \quad (m = 1,\ldots,M). \quad (72)$$

Symmetry of G with respect to interchange of $\mathbf{r}$ and $\mathbf{r}'$ allows us to write

$$\omega_p^2\int_{V_0} d^3\mathbf{r}\psi_m^{in*}(\mathbf{r})\int_{\Delta V} d^3\mathbf{r}'\frac{\partial G}{\partial z\partial z'}\psi_m^{in}(\mathbf{r}') = \omega_p^2\int_{\Delta V} d^3\mathbf{r}\psi_m^{in}(\mathbf{r})\int_{V_0} d^3\mathbf{r}'\frac{\partial G}{\partial z\partial z'}\psi_m^{in*}(\mathbf{r}') = -\omega_m^2\int_{\Delta V} d^3\mathbf{r}\psi_m^{in}(\mathbf{r})\psi_m^{out*}(\mathbf{r}), \quad (73)$$

where in the last step we use Eq. (71) and note that the region ΔV is outside V_0 so that the result of the integration over $\mathbf{r}'$ is ψ_m^{out*}, the outer spheroidal eigenmode. Thus, Eq. (72) becomes

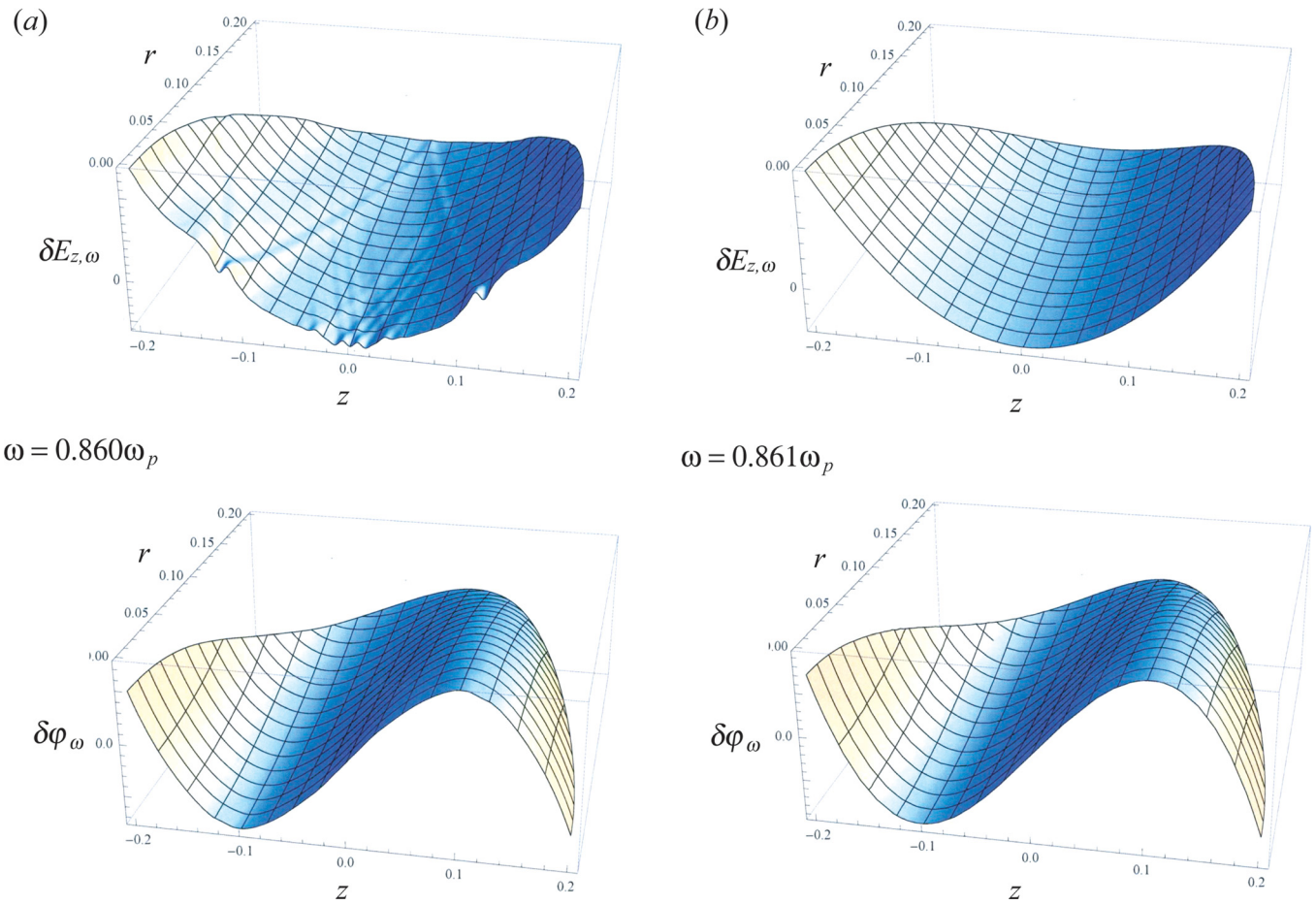

FIG. 9. (Color online) (a) The axial electric field, $\delta E_{z,\omega}$, and potential, $\delta\varphi_\omega$, of a normal mode of a plasma with length $L + \Delta L_0 = 0.401$, radius $a = 0.200$, and end-shape given by $\Delta L_0 = 2a$. Note that this plasma is nearly spherical; the central cylindrical section of the plasma is only one four-thousandth the length of the plasma at $r = 0$. The radius of the trap is $R = 1.0$. (The convergence in the parameter regime $L \ll L_0, a \ll R$ is relatively poor compared with that for long cylindrical plasmas, so the fine-scale ripple in the electric field could be an artifact of the incomplete convergence.) (b) One of two $(l = 3, m = 0)$ modes of a perfectly spherical plasma in the limit $R \to \infty$. Note the similarity between these modes.

$$(\omega^2 - \omega_m^2)a_m = \omega_m^2 \sum_{n=1}^{M} a_n \frac{\int_{\Delta V} d^3\mathbf{r}\psi_n^{in}(\mathbf{r})\psi_m^{out*}(\mathbf{r})}{\int_{V_0} d^3\mathbf{r}\left|\psi_m^{in}(\mathbf{r})\right|^2} \quad (m = 1, \ldots, M). \tag{74}$$

For the case of nondegenerate perturbation theory $(M = 1)$, Eq. (74) implies that

$$\omega^2 - \omega_n^2 = \frac{\omega_n^2 \int_{\Delta V} d^3\mathbf{r}\psi_n^{in}\psi_n^{out*}}{\int_{V_0} d^3\mathbf{r}\left|\psi_n^{in}\right|^2}. \tag{75}$$

TABLE I. Location of cylindrically symmetric $(m = 0)$ spheroidal mode degeneracies with the (1,0) center-of-mass mode (in the range $0 < \alpha < 100$) for $1 < l < 8$.

l	α
4	0.6329
5	2.6295
6(1)	0.1781
6(2)	7.9490
7(1)	0.6261
7(2)	23.4352

For the CM mode, we can check this result by comparison with Eq. (66). To do so, we require the change in shape of the plasma due to an external potential perturbation $\Delta\varphi$ of the form given by Eq. (65). This is worked out in Appendix B. We also require ψ_n^{in} and ψ_n^{out} for the CM mode. According to Eq. (B6), $\psi_n^{in} = 1$, while ψ_n^{out} is given by

$$\psi_n^{out} = \frac{\partial}{\partial_Z}\left[b\xi_2 Q_1^0(\xi_1/d)\right], \tag{76}$$

where $d = \sqrt{b^2 - a^2}$ and ξ_1 and ξ_2 are spheroidal coordinates[7] related to r and z by

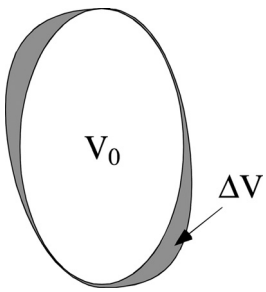

FIG. 10. Perturbed plasma (gray) together with a spheroid of volume V_0 (white) inscribed within the plasma. The small volume difference is ΔV.

$$z = \xi_1\xi_2, \quad r^2 = (\xi_1^2 - d^2)(1 - \xi_2^2), \tag{77}$$

and $Q_1^m(x)$ is an associated Legendre function with branch cuts chosen, so that $Q_1^m(x) \to 0$ as $x \to \infty$. When these results are applied to Eq. (75), we do obtain Eq. (66).

The first order corrections to the eigenfunction are also determined by Eq. (70). Taking an inner product with respect to ψ_n^{in}, where $m = M+1, \ldots, \infty$ yields

$$(\omega^2 - \omega_m^2)\varepsilon_m = \sum_{n=1}^{M} a_n \frac{\omega_m^2 \int_{\Delta V} d^3\mathbf{r}\psi_n^{in}\psi_m^{out^*}}{\int_{V_0} d^3\mathbf{r}|\psi_m^{in}|^2} \quad (m = M+1, \ldots, \infty). \tag{78}$$

Thus, ε_m is small provided that ΔV is small *and* $(\omega^2 - \omega_m^2)/\omega_m^2$ is not small. Of course, this latter condition breaks down at mode degeneracies, which is why, in such cases, any degenerate modes must be included in the set of M modes that have order unity contributions to $\delta E_{z,\omega}$. For degeneracy, the analysis is somewhat simplified by employing orthonormal eigenmodes such that

$$\int_{V_0} d^3\mathbf{r}|\psi^{in}|^2 = 1. \tag{79}$$

Then, for the case of a single degeneracy $(M = 2)$, Eq. (78) implies that

$$(\omega^2 - \omega_1^2 - V_{11})(\omega^2 - \omega_2^2 - V_{22}) = V_{12}V_{21}, \tag{80}$$

where

$$V_{ij} = \omega_i^2 \int_{\Delta V} d^3\mathbf{r}\psi_j^{in}\psi_i^{out^*}. \tag{81}$$

Using Eq. (A16), V_{ij} can be written as

$$V_{ij} = \omega_i^2 \frac{2\pi d}{1-\alpha^2} \sum_n \frac{Q_1^0(b/d)}{Q_n^0(b/d)} A_n \times \int_{-1}^{1} d\xi_2 P_n(\xi_2)\psi_j^{in}(\xi_1 = b, \xi_2)\psi_i^{out*}(\xi_1 = b, \xi_2), \tag{82}$$

where the coefficients A_n are given by Eqs. (A4)–(A10). At degeneracies, we find that $V_{12} = V_{21}^*$ (although away from degeneracy this is not true), so that Eq. (80) predicts real mode frequencies. Note that since V_{ij} is small, the right-hand-side of Eq. (80) can be neglected, except near the degeneracy, where the equation predicts an avoided crossing since $V_{12}V_{21} > 0$. An example is shown for the CM mode in Fig. 11. According to Table I, the CM mode is degenerate with a $(l,m) = (4,0)$ mode when the shape $\alpha = b/a = 0.6329\ldots$. Evaluation of V_{ij}, where $i,j = 1,2$, mode 1 being the CM mode and mode 2 the (4,0) mode, using $\Delta\varphi(r,z)$ given by Eq. (65), implies at $\alpha = 0.6329$,

$$V_{11} = \frac{\omega_z^2 a^2}{R^2}\left(-0.7193\beta_4 + 0.4620\beta_6 \frac{a^2}{R^2} + \cdots\right), \tag{83}$$

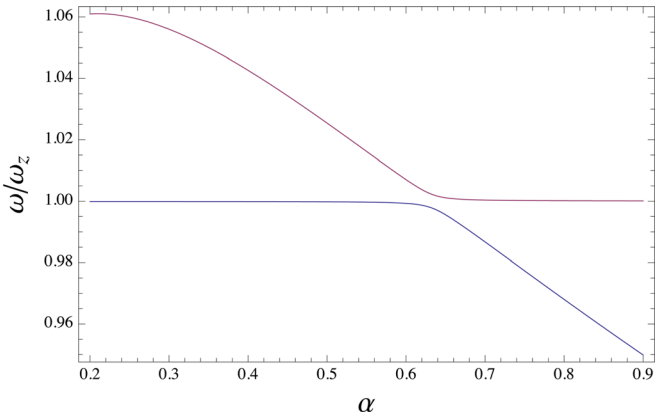

FIG. 11. (Color online) Avoided crossing between CM mode and (4,0) mode taking $\beta_5 = \omega_z^2/100$ and $\beta_n = 0$ for $n \neq 5$.

$$V_{22} = \frac{\omega_z^2 a^2}{R^2}\left(-1.194\beta_4 + 0.6685\beta_6 \frac{a^2}{R^2} + \cdots\right), \tag{84}$$

$$V_{12} = V_{21} = \frac{\omega_z^2 a^3}{R^3}\left(-0.9674\beta_5 + 1.107\beta_7 \frac{a^2}{R^2} + \cdots\right). \tag{85}$$

The resulting frequencies are plotted in Fig. 11 for α near 0.6329, assuming that only β_5 is nonzero. The form of the (1,0) eigenfunction is strongly modified near the degeneracy. According to Eq. (78), at the center of the avoided crossing, the mode δE_z becomes an equal mixture of the (1,0) and (4,0) modes, as shown in Fig. 12. Viscous damping of the

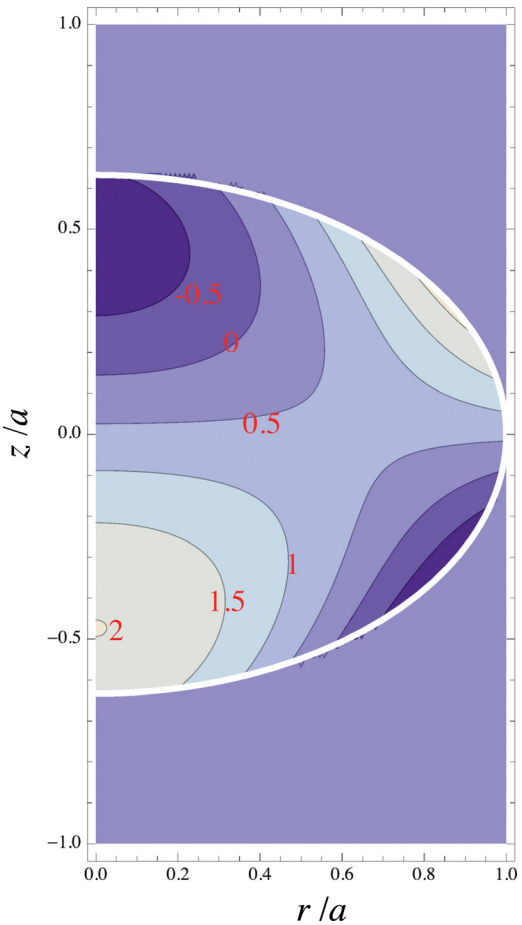

FIG. 12. (Color online) Equal admixture of CM mode and (4,0) mode due to degeneracy where $\alpha = 0.633$.

CM mode would display a strong peak around the degeneracy due to this mixing.

However, there are many other degeneracies with the CM mode and the (4,0) mode over the range of α plotted in the figure. Some of these degeneracies with the CM mode are shown by arrows on the plot. In principle, they would also create avoided crossings, greatly complicating the plot. Since there are a countably infinite number of modes, avoided crossings must occur on a dense set of α values, which could obviate the predictive value of our perturbative approach. However, most of these degeneracies are with modes that have highly disparate spatial scales compared to the low-order CM mode. One can show that if the perturbed value ΔV has a smooth shape, then $V_{ij} \to 0$ as the spatial scales of modes i and j become more disparate. Specifically, for a perturbation by a cylindrically symmetric potential $\Delta\varphi$ given by Eq. (65), if ψ_i is a $(l,0)$ mode and ψ_j is a $(\bar{l},0)$ mode, then the only β_n terms in the potential that contribute to V_{ij} are those with

$$n > l - \bar{l} + 1; \tag{86}$$

and at degeneracy where $V_{ij} = V_{ji}$,

$$n > |l - \bar{l}| + 1. \tag{87}$$

Thus, if $|l - \bar{l}| \gg 1$, only very high-order multipoles $\Delta\varphi$ contribute to V_{ij} In general, Eqs. (A11) and (87) imply that, to lowest order in β_n and a/R,

$$V_{ij} \propto \left(\frac{a}{R}\right)^{|l-\bar{l}|} \beta_{|l-\bar{l}|+2}, \tag{88}$$

for $|l - \bar{l}| \geq 1$. For small β_n and/or a/R and large $|l - \bar{l}|$, this implies that the avoided crossings are extremely narrow and can be neglected.

VII. VISCOUS DAMPING

In the low-temperature regime that we have in mind, the phase velocity of any traveling wave comprising a mode is large in comparison to the thermal velocity, so Landau damping is negligible. Instead, the modes are damped by viscosity. (The contribution to the damping from heat conduction is higher order in the ratio of the thermal velocity to the phase velocity, so we ignore this contribution here.[16])

Here, we calculate an expression for the viscous damping rate, assuming that the damping is weak, so that perturbation theory can be used. With viscosity included, the momentum equation (12) takes the form

$$-i\omega m n_0 \delta V_{z,\omega} = -q n_0 \frac{\partial \delta\varphi_\omega}{\partial z} + \frac{1}{r}\frac{\partial}{\partial r}\left(r m n_0 \zeta_\perp \frac{\partial \delta V_{z,\omega}}{\partial r}\right) + \frac{4}{3}\frac{\partial}{\partial z}\left(m n_0 \zeta_\parallel \frac{\partial \delta V_{z,\omega}}{\partial r}\right), \tag{89}$$

where $\zeta_\perp$ is the cross-field kinematic viscosity and $\zeta_\parallel$ is the parallel kinematic viscosity. Poisson's equation (10) and the continuity equation (11) remain unchanged. We define the parameters $\alpha_\parallel \equiv \zeta_z/(\omega L_\parallel^2)$ and $\alpha_\perp \equiv \zeta_\perp/(\omega L_\parallel^2)$, where $L_\parallel$ and $L_\perp$ are the axial and transverse scale-lengths of the mode. For a weakly damped mode, these are small parameters. We thus expand the mode and its frequency as perturbation series, keeping only terms of zero- and first-order in $\alpha_\parallel$ and $\alpha_\perp$: $\delta n_\omega \cong \delta n_\omega^{(0)} + \delta n_\omega^{(1)}$; $\delta V_{z,\omega} \cong \delta V_{z,\omega}^{(0)} + \delta V_{z,\omega}^{(1)}$; $\delta\varphi_\omega \cong \delta\varphi_\omega^{(0)} + \delta\varphi_\omega^{(1)}$; and $\omega \cong \omega^{(0)} - i\gamma^{(1)}$. Together $\delta n_\omega^{(0)}$, $\delta V_{z,\omega}^{(0)}$, and $\delta\varphi_\omega^{(0)}$ satisfy the inviscid fluid equations for a mode with frequency $\omega^{(0)}$. To first order, the viscous momentum equation (89) can be rewritten as

$$-i\omega m n_0(\delta V_\omega^{(0)} + \delta V_\omega^{(1)}) = -q n_0 \frac{\partial}{\partial z}(\delta\varphi_\omega^{(0)} + \delta\varphi_\omega^{(1)}) + \frac{1}{r}\frac{\partial}{\partial r}\left[r m n_0 \zeta_\perp \frac{\partial}{\partial r}\left(\frac{q}{i\omega}\frac{\partial \delta\varphi_\omega^{(0)}}{\partial z}\right)\right] + \frac{4}{3}\frac{\partial}{\partial z}\left[n_0 \zeta_\parallel \frac{\partial}{\partial z}\left(\frac{q}{i\omega}\frac{\partial \delta\varphi_\omega^{(0)}}{\partial z}\right)\right]. \tag{90}$$

Insertion of this expression into the continuity equation (11) gives δn_ω in terms of $\delta\varphi_\omega$. Poisson's equation then becomes

$$\begin{aligned}\frac{1}{r}\frac{\partial}{\partial r} r \frac{\partial \delta\varphi_\omega^{(1)}}{\partial r} + \frac{\partial^2 \delta\varphi_\omega^{(1)}}{\partial z^2} &= \frac{\partial}{\partial z}\left(\frac{\omega_p^2}{\omega^{(0)2}}\frac{\partial \delta\varphi_\omega^{(1)}}{\partial z}\right) + \frac{\partial}{\partial z}\left(\frac{2\omega_p^2 i\gamma^{(1)}}{\omega^{(0)3}}\frac{\partial \delta\varphi_\omega^{(0)}}{\partial z}\right) \\ &+ \frac{\partial}{\partial z}\left\{\frac{1}{r}\frac{\partial}{\partial r}\left[r\frac{i\omega_p^2\zeta_\perp}{\omega^{(0)3}}\frac{\partial}{\partial r}\left(\frac{\partial \delta\varphi_\omega^{(0)}}{\partial z}\right)\right]\right\} \\ &+ \frac{4}{3}\frac{\partial^2}{\partial z^2}\left(\frac{i\omega_p^2\zeta_\parallel}{\omega^{(0)3}}\frac{\partial \delta\varphi_\omega^{(0)}}{\partial z^2}\right).\end{aligned} \tag{91}$$

Here, we have used the fact that $\delta\varphi_\omega^{(0)}$ and $\omega^{(0)}$ together satisfy the inviscid mode equation (13), which implies that the zero-order terms cancel. Multiplying Eq. (91) by $\delta\varphi_\omega^{(0)}$, integrating over the entire domain of the trap, and integrating each term by parts twice eliminate the terms involving $\delta\varphi_\omega^{(1)}$ [again, by virtue of Eq. (13)], and we are left with an expression for the first-order viscous correction to the frequency in terms of the inviscid approximation to the mode,

$$\gamma^{(1)} = \frac{\int r dr dz \omega_p^2(r,z)\left[(2\zeta_\parallel/3)(\partial\delta E_{z,\omega}^{(0)}/\partial z)^2 + (\zeta_\perp/2)(\partial\delta E_{z,\omega}^{(0)}/\partial r)^2\right]}{\int r dr dz \omega_p^2(r,z)\delta E_{z,\omega}^{(0)2}}, \tag{92}$$

where $\delta E_{z,\omega}^{(0)} = -\partial\delta\varphi_{\omega}^{(0)}/\partial z$. This expression is purely real and non-negative and gives the viscous damping rate of the mode.

Due to the mixing of degenerate waves, the axial and transverse scale-lengths, $L_{\|}$ and $L_{\perp}$ of even the least-damped modes can be much smaller than the corresponding dimensions of the plasma. As a result, the damping of these modes is significantly greater than one would predict based on the single-wave approximation,[12,14,16] which takes the mode potential inside the plasma to be given by a single Trivelpiece-Gould wave with wavenumber $k_m = m\pi/L$ $[1 - O(R/L)]$. For example, according to Eq. (92), the mode displayed in Fig. 8(a) damps at the rate $\gamma = (27.0\zeta_{\perp} + 0.325\zeta_{\|})/R^2$. By comparison, if this mode is approximated by its largest-amplitude Trivelpiece-Gould component ($m = 1$, in this case), the smaller rate $\gamma = (2.94\zeta_{\perp} + 0.0930\zeta_{\|})/R^2$ is obtained.

VIII. SUMMARY

We have calculated several azimuthally symmetric, longitudinal normal modes of a cold, magnetized single-species plasma column. Each normal mode is not a standing Trivelpiece-Gould wave with well-defined wavenumber but is instead a more complicated superposition of many such waves, often exhibiting sharp features along the resonance cones corresponding to the mode frequency. We have also analyzed the mixing of Dubin modes on a cold, magnetized plasma of nearly spheroidal shape, using perturbation theory. We find that a slight deviation of the plasma boundary from the spheroidal shape can induce strong mixing between multiple Dubin modes when the aspect ratio is such that these modes are degenerate. The mixing effects described here occur only when the Debye length is small in comparison with the scale-lengths characteristic of the mode. In this cold-fluid regime, the modes are damped by viscosity, and this damping is enhanced by the presence of large wavenumbers in the admixture for the mode.

ACKNOWLEDGMENTS

The authors wish to thank Matthew Affolter, Francois Anderegg, Fred Driscoll, and Ross Spencer for many useful discussions. This research was supported by grants from NSF (No. PHY-0903877) and DOE (No. DE-SC0002451).

APPENDIX A: PERTURBATION OF A SPHEROIDAL PLASMA BOUNDARY

In this appendix, we evaluate the change in plasma shape created by an external potential perturbation $\Delta\varphi$ given by Eq. (65). This potential can also be written in cylindrical coordinates (ρ, z) as

$$q\Delta\varphi_{ext}(r,z) = \frac{1}{2}m\omega_2^2\left[\frac{\beta_3}{R}z\left(z^2 - \frac{3}{2}r^2\right) + \frac{\beta_4}{R^2}\left(z^4 - 3z^2r^2 + \frac{3}{8}r^4 + \cdots\right)\right]. \quad \text{(A1)}$$

Within the plasma, this potential is cancelled by a space-charge potential $\Delta\varphi_p^{in}$ due to the change in shape,

$$\Delta\varphi_p^{in} = -\Delta\varphi_{ext}. \quad \text{(A2)}$$

Since $\Delta\varphi_p^{in}$ is due to a small change in shape, it is a solution of Laplace's equation due to a surface charge distribution caused by the shape change. This effect is most easily described in spheroidal coordinates (ξ_1, ξ_2). In these coordinates, inside the plasma, the cylindrically symmetric solution to Laplace's equation is

$$q\Delta\varphi_p^{in} = -m\omega_2^2\sum_n A_n P_n(\xi_1/d)P_n(\xi_2), \quad \text{(A3)}$$

where the coefficients A_n are determined by Eqs. (A1) and (A2),

$$A_1 = \frac{d^3}{2R}\left(\frac{3}{5}\beta_3 + \frac{3}{7}\beta_5\frac{d^2}{R^2} + \frac{1}{3}\beta_7\frac{d^4}{R^4} + \cdots\right), \quad \text{(A4)}$$

$$A_2 = \frac{d^4}{21R^2}\left(6\beta_4 + 5\beta_6\frac{d^2}{R^2} + \cdots\right), \quad \text{(A5)}$$

$$A_3 = \frac{d^3}{R}\left(\beta_3 + \frac{2}{9}\beta_5\frac{d^2}{R^2} + \frac{7}{33}\beta_7\frac{d^4}{R^4} + \cdots\right), \quad \text{(A6)}$$

$$A_4 = \frac{4d^4}{385R^2}\left(11\beta_4 + 15\beta_6\frac{d^2}{R^2} + \cdots\right), \quad \text{(A7)}$$

$$A_5 = \frac{4d^5}{R^3}\left(\frac{\beta_5}{63} + \frac{\beta_7}{39}\frac{d^2}{R^2} + \cdots\right), \quad \text{(A8)}$$

$$A_6 = \frac{8d^6}{231R^4}(\beta_6 + \cdots), \quad \text{(A9)}$$

$$A_7 = \frac{8d^7}{429R^5}(\beta_7 + \cdots), \quad \text{(A10)}$$

$$A_n \propto \frac{d^n}{R^{n-2}}(\beta_n + \cdots). \quad \text{(A11)}$$

Outside the plasma, the Laplace solution is

$$q\Delta\varphi_p^{out} = -m\omega_z^2\sum_n B_n Q_n^0(\xi_1/d)P_n(\xi_2). \quad \text{(A12)}$$

The outer and inner solutions are connected by the change in shape of the plasma boundary, which can be described as a curve $\xi_1(\xi_2) = b + \Delta\xi_1(\xi_2)$, where $\Delta\xi_1(\xi_2)$ is given by

$$\Delta\xi_1(\xi_2) = \sum_n \frac{C_n P_n(\xi_2)}{b^2 - d^2\xi_2^2}. \quad \text{(A13)}$$

The coefficients C_n are determined by the solution to

$$\nabla^2\Delta\varphi_p = -4\pi e n_0 \Delta\xi_1\delta(\xi_1 - b), \quad \text{(A14)}$$

where n_0 is the plasma density; the right-hand side represents the surface charge due to the shape change. Using Eqs. (A12) and (A13) in Eq. (A14) and matching potentials across the boundary yields

$$C_n = -\frac{\omega_z^2}{\omega_p^2}\frac{d}{Q_n^0(b/d)}A_n = -\frac{Q_1^0(b/d)}{Q_n^0(b/d)}\frac{d}{\alpha^2 - 1}A_n, \quad \text{(A15)}$$

where ω_p is the plasma frequency, and we have used the well-known relation between ω_z and ω_p for plasma

spheroids, Eq. (B5). Note that the coefficients A_n, B_n, and C_n appearing in these appendices are not the same as those appearing in Secs. IV and V.

Finally, in order to complete integrals over ΔV appearing in $V_{ij,}$ we note that

$$\int_{\Delta V} d^3\mathbf{r} = \int_0^{2\pi} d\phi \int_{-1}^{1} d\xi_2 \left(b^2 - d^2\xi_2^2\right)\Delta\xi_1(\xi_2) = \frac{d}{1-\alpha^2}\sum_n \frac{Q_1^0(b/d)}{Q_n^0(b/d)} A_n \int_0^{2\pi} d\phi \int_{-1}^{1} d\xi_2 P_n(\xi_2), \tag{A16}$$

where we have used Eqs. (A13) and (A15).

APPENDIX B: NORMAL MODES OF A MAGNETIZED SPHEROIDAL PLASMA

In this appendix, we collect several known results for normal modes of a magnetized spheroid. In the $B \to \infty$ limit, the dispersion relation for the magnetized plasma modes is

$$\varepsilon = \left(\frac{\alpha^2 - \varepsilon_3}{\alpha^2 - 1}\right)^{1/2} \frac{P_l^m Q_l^{m'}}{P_l^{m'} Q_l^m}, \tag{B1}$$

where $\varepsilon_3 = 1 - \omega_p^2/\omega^2$, $P_l^m = P_l^m(\alpha/(\alpha^2-\varepsilon_3)^{1/2})$, and $Q_l^m = Q_l^m(\alpha/(\alpha^2-\varepsilon_3)^{1/2})$.

Mode potentials inside and outside the spheroid are

$$\delta\varphi^{in} = P_l^m\left(\bar{\xi}_1/\bar{d}\right)P_l^m\left(\bar{\xi}_2\right)e^{im\phi}, \tag{B2}$$

$$\delta\varphi^{out} = \frac{P_l^m(\bar{b}/\bar{d})}{Q_l^m(b/d)} P_l^m(\xi_1/d)P_l^m(\xi_2)e^{im\phi}, \tag{B3}$$

where $\bar{b} = b/\sqrt{\varepsilon_3}$, $\bar{d} = \sqrt{\bar{b}^2 - a^2}$, and $\left(\bar{\xi}_1, \bar{\xi}_2\right)$ are modified spheroidal coordinates defined by

$$z = \bar{\xi}_1\bar{\xi}_2\sqrt{\varepsilon_{3,}} \quad r^2 = (\bar{\xi}_1^2 - \bar{d}^2)(1 - \bar{\xi}_2^2). \tag{B4}$$

Equation (B1) can be written as a polynomial in ω^2 with $\mathrm{Int}[(l-m+1)/2]$ real positive solutions for ω^2. The inner potential $\partial\varphi_{in}$ can also be written as a multinomial in r and z of order l (multiplied by $e^{im\phi}$). The eigenfunctions ψ_n used in Sec. VI are proportional to $\partial\varphi/\partial z$.

For the (1,0) mode, Eqs. (B1) and (B2) simplify to

$$\frac{\omega_z^2}{\omega_p^2} = \frac{Q_1^0(b/d)}{\alpha^2 - 1}, \tag{B5}$$

$$\delta\varphi^{in} = z. \tag{B6}$$

There are two (4,0) plasma modes, with frequencies given by solutions to the polynomial equation

$$\omega^4\left[8\alpha^4(\gamma-10) + 12\alpha^2(2\gamma-5) + 3\gamma\right] + 2\omega^2\omega_p^2\left[40\alpha^4 - 12\alpha^2(\gamma-5) - 3\gamma\right] + 3\omega_p^4(\gamma - 20\alpha^2) = 0, \tag{B7}$$

where

$$\gamma = \frac{bQ_4^{0\prime}(b/d)}{dQ_4^0(b/d)}. \tag{B8}$$

For both modes, the inner potential is

$$\delta\varphi^{in} = 280z^4 + 105\varepsilon_3^2 r^4 - 120z^2\left[7\varepsilon_3 r^2 + 2(b^2 - \varepsilon_3 a^2)\right] + 120\varepsilon_3 r^2(b^2 - \varepsilon_3 a^2) + 24(b^2 - \varepsilon_3 a^2)^2. \tag{B9}$$

[1]J. S. deGrassie and J. H. Malmberg, Phys. Rev. Lett. **39**, 1077 (1977).
[2]D. H. E. Dubin and T. M. O'Neil, Rev. Mod. Phys. **71**, 87 (1999).
[3]S. A. Prasad and T. M. O'Neil, Phys. Fluids **22**, 278 (1979).
[4]R. K. Fisher and R. W. Gould, Phys. Rev. Lett. **22**, 1093 (1969).
[5]F. Anderegg, C. F. Driscoll, D. H. E. Dubin, and T. M. O'Neil, Phys. Plasmas **17**, 055702 (2010).
[6]L. R. Brewer, J. D. Prestage, J. J. Bollinger, W. M. Itano, D. J. Larson, and D. J. Wineland, Phys. Rev. A **38**, 859 (1988).
[7]D. H. E. Dubin, Phys. Rev. Lett. **66**, 2076 (1991).
[8]T. B. Mitchell, J. J. Bollinger, X.-P. Huang, and W. M. Itano, Opt. Express **2**, 314 (1998).
[9]A. W. Trivelpiece and R. W. Gould, J. Appl. Phys. **30**, 1784 (1959).
[10]J. R. Danielson, F. Anderegg, and C. F. Driscoll, Phys. Rev. Lett. **92**, 245003 (2004).
[11]S. A. Prasad and T. M. O'Neil, Phys. Fluids **26**, 665 (1983).
[12]J. K. Jennings, R. L. Spencer, and K. C. Hansen, Phys. Plasmas **2**, 2630 (1995).
[13]D. H. E. Dubin, Phys. Plasmas **12**, 042107 (2005).
[14]S. N. Rasband and R. L. Spencer, Phys. Plasmas **10**, 948 (2003).
[15]D. H. E. Dubin, Phys. Rev. E **53**, 5268 (1996).
[16]M. W. Anderson and T. M. O'Neil, Phys. Plasmas **14**, 112110 (2007).